Systems/Circuits

Neuropeptide Y Signaling Regulates Recurrent Excitation in the Auditory Midbrain

Marina A. Silveira,[1] Audrey C. Drotos,[1] Trinity M. Pirrone,[1,2] Trevor S. Versalle,[1] Amanda Bock,[1] and Michael T. Roberts[1,3]

[1]Kresge Hearing Research Institute, Department of Otolaryngology–Head and Neck Surgery, University of Michigan, Ann Arbor, Michigan 48109, [2]Macalester College, St. Paul, Minnesota 55105, and [3]Department of Molecular and Integrative Physiology, University of Michigan, Ann Arbor, Michigan 48109

Neuropeptides play key roles in shaping the organization and function of neuronal circuits. In the inferior colliculus (IC), which is in the auditory midbrain, Neuropeptide Y (NPY) is expressed by a class of GABAergic neurons that project locally and outside the IC. Most neurons in the IC have local axon collaterals; however, the organization and function of local circuits in the IC remain unknown. We previously found that excitatory neurons in the IC can express the NPY Y_1 receptor (Y_1R^+) and application of the Y_1R agonist, [Leu^{31}, Pro^{34}]-NPY (LP-NPY), decreases the excitability of Y_1R^+ neurons. As NPY signaling regulates recurrent excitation in other brain regions, we hypothesized that Y_1R^+ neurons form interconnected local circuits in the IC and that NPY decreases the strength of recurrent excitation in these circuits. To test this hypothesis, we used optogenetics to activate Y_1R^+ neurons in mice of both sexes while recording from other neurons in the ipsilateral IC. We found that nearly 80% of glutamatergic IC neurons express the Y_1 receptor, providing extensive opportunities for NPY signaling to regulate local circuits. Additionally, Y_1R^+ neuron synapses exhibited modest short-term synaptic plasticity, suggesting that local excitatory circuits maintain their influence over computations during sustained stimuli. We further found that application of LP-NPY decreased recurrent excitation in the IC, suggesting that NPY signaling strongly regulates local circuit function in the auditory midbrain. Our findings show that Y_1R^+ excitatory neurons form interconnected local circuits in the IC, and their influence over local circuits is regulated by NPY signaling.

Key words: **auditory; inferior colliculus; local circuits; neuromodulation; neuropeptide Y; optogenetics**

Significance Statement

Local networks play fundamental roles in shaping neuronal computations in the brain. The IC, localized in the auditory midbrain, plays an essential role in sound processing, but the organization of local circuits in the IC is largely unknown. Here, we show that IC neurons that express the Neuropeptide Y_1 receptor (Y_1R^+ neurons) make up most of the excitatory neurons in the IC and form interconnected local circuits. Additionally, we found that NPY, which is a powerful neuromodulator known to shape neuronal activity in other brain regions, decreases the extensive recurrent excitation mediated by Y_1R^+ neurons in local IC circuits. Thus, our results suggest that local NPY signaling is a key regulator of auditory computations in the IC.

Introduction

Local circuits play a critical role in encoding, amplifying, and transforming inputs in the brain (Saka et al., 2002; Burke et al., 2017; Geiller et al., 2022). In the auditory midbrain, the inferior colliculus (IC) contains an extensive network of local axons formed by both excitatory and inhibitory neurons (Oliver et al., 1991; Sturm et al., 2014, 2017; Ito et al., 2016). The IC acts as a hub in the central auditory pathway (Adams, 1979; Cant and Benson, 2006, 2007), integrating and transforming many ascending and descending inputs and, in turn, providing major projections to the thalamocortical system and auditory brainstem (Winer et al., 1996; Peruzzi et al., 1997; Goyer et al., 2019; Kreeger et al., 2021; Anair et al., 2022). Although anatomic reports indicate that most neurons in the IC have local axon collaterals (Oliver et al., 1991; Ito et al., 2016), most studies have focused on understanding the long-range projections of IC neurons. Thus, the organization and function of local IC circuits remain poorly understood.

The main barrier to understanding the function and organization of local IC circuits is that it was not possible to identify

Received May 16, 2023; revised Sep. 5, 2023; accepted Sep. 6, 2023.

Author contributions: M.A.S. and M.T.R. designed research; M.A.S., A.C.D., T.M.P., T.S.V., and A.B. performed research; M.A.S., A.C.D., T.M.P., and M.T.R. analyzed data; M.A.S. and M.T.R. wrote the paper.

This work was supported by National Institutes of Health Grants K99 DC019415 (M.A.S.) and R01 DC018284 (M.T.R.), National Science Foundation (NSF) Graduate Research Fellowship Program Grant DGE 1256260 (A.C.D.), and NSF Grant 2243919 (T.M.P.). We thank Bo Duan, Susan Shore, and Pierre Apostolides for discussions and advice and Yoani Herrera for help with diagrams.

The authors declare no competing financial interests.

Correspondence should be addressed to Marina A. Silveira at marina.silveira@utsa.edu.

https://doi.org/10.1523/JNEUROSCI.0900-23.2023

and manipulate specific classes of IC neurons (Peruzzi et al., 2000; Palmer et al., 2013; Beebe et al., 2016). However, in the past few years two classes of molecularly distinct glutamatergic neurons have been identified, vasoactive intestinal peptide (VIP; Goyer et al., 2019) and cholecystokinin (CCK; Kreeger et al., 2021). Additionally, we discovered that Neuropeptide Y (NPY) is expressed in the IC and is a molecular marker for a large class of GABAergic principal neurons (Silveira et al., 2020).

NPY is a powerful neuromodulator known in other brain regions to work in concert with GABA to shape neuronal activity (Colmers and Bleakman, 1994; Bacci et al., 2002; van den Pol, 2012; Gøtzsche and Woldbye, 2016; Li et al., 2017). By acting on the NPY Y family of G-protein-coupled receptors, NPY can regulate neurotransmitter release from presynaptic neurons (Sun et al., 2001a; Bacci et al., 2002) or modulate excitability in postsynaptic targets. NPY is thereby able to reconfigure neuronal circuit activity by modulating ion channels such as G protein-gated inwardly rectifying potassium (GIRK) (Sun et al., 2001b) and hyperpolarization-activated cyclic nucleotide-gated (HCN) channels (Giesbrecht et al., 2010). This suggests the intriguing possibility that NPY signaling regulates auditory processing across spatial and temporal scales, which is not possible with GABAergic signaling alone. Indeed, we previously showed that a subset of glutamatergic neurons in the IC express the NPY Y_1R receptor (Y_1R^+), and application of the Y_1R agonist [Leu^{31}, Pro^{34}]-NPY (LP-NPY) led to hyperpolarization of Y_1R^+ neurons (Silveira et al., 2020). Y_1R^+ neurons are thought to be glutamatergic neurons because they do not express the GABA-synthetic enzyme GAD67, and they likely encompass more than one class of glutamatergic neurons as they exhibit heterogenous intrinsic physiology (Silveira et al., 2020).

Because most IC neurons have local axon collaterals (Oliver et al., 1991), we hypothesized that Y_1R^+ neurons form interconnected local circuits that can drive recurrent excitation in the IC (Oliver et al., 1991). As NPY inhibits recurrent activity in hippocampus (Tu et al., 2005), we further hypothesized that Y_1R^+ circuits in the IC are subject to NPY modulation. To test these hypotheses, we used whole-cell patch-clamp recordings and optogenetics in brain slices from Y_1R-Cre x Ai14 mice, in which Y_1R^+ neurons are identified by tdTomato expression. Our data reveal that 78.4% of glutamatergic neurons in the IC express *Npy1r* mRNA and that Y_1R^+ neurons provide excitatory input to many other neurons in the local IC. Y_1R^+ synapses onto other IC neurons exhibited little short-term synaptic plasticity, suggesting a consistent influence of Y_1R^+ neurons during sustained computations in IC circuits. In addition, we found that activation of Y_1R^+ neurons drove recurrent excitation in IC circuits that was inhibited by LP-NPY. Together, our results reveal that Y_1R^+ neurons in the IC form interconnected local circuits and that the excitability of these circuits is regulated by NPY signaling. Thus, we propose that NPY signaling is a major modulator of the auditory computations performed by local circuits in the auditory midbrain.

Materials and Methods

Animals. The experiments performed here were approved by the University of Michigan Institutional Animal Care and Use Committee and were in accordance with National Institutes of Health *Guide for the Care and Use of Laboratory Animals.* Mice had *ad libitum* access to food and water and were maintained on a 12 h day/night cycle. $Npy1r^{cre}$ mice (B6.*Cg-Npy1r*$^{tm1.1(cre/GFP)Rpa}$, stock # 030544, The Jackson Laboratory; Padilla et al., 2016), were crossed with Ai14 Cre-reporter mice (B6.Cg-*Gt(ROSA)26Sor*$^{tm14(CAG-tdTomato)}$*Hze*; stock # 007914, The Jackson Laboratory; Madisen et al., 2010) to allow identification of Y_1R^+ neurons by tdTomato fluorescence (Y_1R-Cre x Ai14). Both mouse lines were on a C57BL/6J background. Because C57BL/6J mice are subject to age-related hearing loss because of the *Cdh23*^{ahl} mutation, experiments were performed in mice postnatal day (P)24–P82 to avoid potential effects of age-related hearing loss (Noben-Trauth et al., 2003). Mice of either sex were used for all experiments.

RNAScope in situ hybridization assay and analysis. Two *in situ* hybridization assays were performed. For both assays, we used the RNAScope Multiplex Fluorescence V2 kit (catalog #320850, Advanced Cell Diagnostics; Wang et al., 2012). Brain slices were prepared using the fresh-frozen method. Mice were deeply anesthetized with isoflurane, and brains from three mice (two males and one female Y_1R-Cre x Ai14, P59, for assay 1 and two females and one male C57BL/6J, P55, for assay 2) were quickly dissected, frozen in dry ice, and maintained at −80°C until it was time to slice. Before slicing, brains were equilibrated at −20°C for 1 h, and 15 µm sections were collected using a cryostat and mounted on Superfrost Plus slides (catalog #22037246, Thermo Fisher Scientific). RNAScope assays were performed following the recommendations of the manufacturer. In brief, slices were fixed in 10% neutral buffered formalin (catalog #HT501128, Sigma-Aldrich), dehydrated in increasing concentrations of ethanol, followed by drawing a hydrophobic barrier around the sections. Next, hydrogen peroxide was used to block endogenous peroxidase. For hybridization, we used the following combinations of probes: (1) *tdTomato*, *Vglut2* and *Npy1r* and (2) *VIP*, *CCK*, and *Npy1r*. RNAscope probes have high sensitivity and specificity and are therefore routinely used for comparing expression of different mRNAs within a single assay (Wang et al., 2012). All probes, positive controls, and negative controls were incubated for 2 h followed by the amplification (AMP 1–3) step. After the signal was developed using the appropriate HRP, Opal dyes (1:1000) were assigned for each channel as follows: Assay 1, *tdTomato* expression was identified by Opal 690 (catalog #FP1497001KT, Akoya Bioscience), *Vglut2* expression was identified by Opal 570 (catalog #FP1488001KT, Akoya Bioscience), and *Npy1r* expression was identified by Opal 520 (catalog #FP1487001KT, Akoya Bioscience); assay 2, *VIP* expression was identified by Opal 520 (catalog #FP1487001KT, Akoya Bioscience), *CCK* expression was identified by Opal 570 (catalog #FP1488001KT, Akoya Bioscience), and *Npy1r* expression was identified by Opal 690 (catalog #FP1497001KT, Akoya Bioscience). Following staining with DAPI, slices were coverslipped using ProLong Gold Antifade Mountant (catalog #P36934, Thermo Fisher Scientific). Images were collected within 2 weeks after the assay. Representative sections (including caudal, midrostrocaudal, and rostral, three sections per mouse) were imaged using a 0.75 NA 20× objective at 2-µm-depth intervals on a Leica TCS SP8 laser scanning confocal microscope (Leica Microsystems). For the validation of the mouse line (assay 1), quantification was performed manually using Fiji software (ImageJ, National Institutes of Health; Schindelin et al., 2012). A grid was randomly placed over every image, and quantification was performed every fourth to sixth grid square using the multipoint tool by placing a marker on the top of each cell. Channels of each color were quantified separately to avoid bias. To test whether *Npy1r*-expressing neurons express *VIP* and/or *CCK* (assay 2) we looked for representative examples of cells expressing a combination of the three different mRNAs.

Intracranial virus injection. To investigate the function of IC local circuits, 17 Y_1R-Cre x Ai14 mice (9 males and 8 females) were injected in the right IC with the recombinant adeno-associated virus rAAV1-hSyn-FLEX-Chronos-GFP (lot #AV6551B, University of North Carolina Vector Core; titer 2.8×10^{12} vg/ml; plasmid #62722, Addgene; Klapoetke et al., 2014). For short-term synaptic plasticity experiments and recurrent excitation experiments, 25 Y_1R-Cre x Ai14 mice (14 males and 11 females) were injected in the right IC with either rAAV1-hSyn-FLEX-Chronos-GFP or rAAV9-CAG-DIO-ChroME-ST-P2A-H2B-mRuby3 (titer ranging from 2.7×1012-2.7×10^{13} gc/ml; #108912, Addgene; Mardinly et al., 2018). Surgeries were performed using standard aseptic techniques in males and females, aged P25–P68, as previously described (Goyer et al., 2019; Silveira et al., 2020). In brief, mice were deeply anesthetized using 3% isoflurane and placed in a stereotaxic base with a homeothermic heating pad to maintain body temperature. For the remainder of the surgery, isoflurane was dropped to 1–2%, and breathing

pattern was monitored. Carprofen (5 mg/kg; CarproJect, Henry Schein Animal Health) was injected subcutaneously. After exposing the skull with a rostrocaudal incision, a unilateral craniotomy was performed in the right IC using a micromotor drill (K.1050, Foredom Electric) with a 0.5 mm burr (Fine Science Tools). Injections were made in two penetrations using coordinates defined relative to lambda and relative to the surface of the skull (injection 1, 900 µm caudal, 1000 µm lateral, and 1800 µm deep; injection 2, 900 µm caudal, 1200 µm lateral, and 1800 µm deep). Glass capillaries used for injections (catalog #3-000-203-G/X, Drummond Scientific) were pulled with a P-1000 microelectrode puller (Sutter Instrument). The injection tip was back filled with mineral oil and front filled with the virus of interest. The amount of virus injected ranged from 50 to 300 nl; however, most mice were injected with 100 nl of virus. At the end of the procedure, the scalp was sutured using Ethilon size 6-0 (0.7 metric) nylon sutures (Ethicon). The analgesic lidocaine hydrochloride (2%, 0.5 ml; Akorn) was applied to the incision. Mice were monitored for 10 d. Electrophysiological recordings were performed 2–4 weeks after the injection.

Brain slice preparation. To characterize the intrinsic physiology of Y_1R^+ neurons and to evaluate local projections mediated by Y_1R^+ neurons, we performed whole-cell patch-clamp recordings targeted to either Y_1R^+ or Y_1R^- neurons that were identified in Y_1R-Cre x Ai14 mice by the presence or lack of tdTomato expression. To prepare brain slices, mice were decapitated after being deeply anesthetized with isoflurane. The brain was carefully removed, and the IC was dissected in 34°C ACSF containing the following (in mM): 125 NaCl, 12.5 glucose, 25 $NaHCO_3$, 3 KCl, 1.25 NaH_2PO_4, 1.5 $CaCl_2$, 1 $MgSO_4$, 3 sodium pyruvate, and 0.40 L-ascorbic acid. ACSF was bubbled to a pH of 7.4 with 5% CO_2 in 95% O_2 for at least 30 min before dissection. Coronal IC slices (200 µm) were prepared using a vibrating microtome (VT1200 S, Leica Biosystems). Slices were incubated at 34°C for 30 min in ACSF bubbled with 5% CO_2 in 95% O_2. Unless otherwise noted, all reagents were obtained from Thermo Fisher Scientific.

Electrophysiological recordings. For whole-cell current-clamp and voltage-clamp recordings, slices were transferred to a bath chamber that was continuously perfused with 34–35°C ACSF bubbled with 5% CO_2 in 95% O_2 at 2 ml/min. Y_1R^+ and Y_1R^- neurons were identified with epifluorescence using a Nikon FN1 microscope or an Olympus BX51WI microscope. Recording pipettes were pulled using a P-1000 microelectrode puller (Sutter Instrument) from borosilicate glass capillaries (outer diameter 1.5 mm, inner diameter 0.86 mm; catalog #BF150-86–10, Sutter Instrument). Internal solution to fill the pipettes contained the following (in mM): 115 K-gluconate, 7.73 KCl, 0.5 EGTA, 10 HEPES, 10 Na_2-phosphocreatine, 4 MgATP, 0.3 NaGTP, and 0.1% biocytin (w/v). The pH was adjusted to 7.3 with KOH and osmolality to 290 mmol/kg with sucrose. Pipettes with resistances from 2.5 to 5.5 MΩ were used for recordings.

Whole-cell current-clamp recordings were performed using a BVC-700A amplifier (Dagan). Data were acquired using custom software written in Igor Pro, low-pass filtered at 10 kHz, and sampled at 50 kHz with a National Instruments PCIe-6343 data acquisition board. Pipette capacitance and series resistance were corrected using the bridge balance circuitry of the BVC-700A amplifier. Recordings with series resistance >20 MΩ and recordings with series resistance that changed >15% were not included in analysis. To assess input resistance, a series of 100 ms current steps that hyperpolarized the membrane potential from just below rest to −100 mV was applied. The peak and steady-state voltage responses were calculated for each step. A voltage versus current plot was generated, and the peak and steady-state input resistances were calculated based on the slope of a linear fit. To calculate the membrane time constant, 50 100–300 ms current steps that resulted in 2–6 mV membrane hyperpolarization were applied. Membrane time constant was obtained by fitting an exponential function to each response and obtaining the median τ. Liquid junction potential was −11 mV and was corrected in all cases.

Whole-cell voltage-clamp recordings were made using an AxoPatch 200A amplifier. Series resistance compensation was performed using 70–80% prediction and correction. Recordings with series resistance >20 MΩ or that changed >15% during the recording were not included in the final analysis. The internal solution was the same as the one used for current-clamp experiments, and recordings were performed at −81 mV with the liquid junction potential of −11 mV corrected in all cases.

Channelrhodopsin-assisted circuit mapping. After injections, we allowed 2–4 weeks for Chronos or ChroME expression. Brain slices were prepared, and recordings were performed under red light to limit Chronos or ChroME activation. Recordings were targeted to Y_1R^+ or Y_1R^- neurons, and the identification of neurons was done as fast as possible to avoid activation of optogenetic opsins. Chronos or ChroME was activated by brief pulses of 470 nm light emitted by a blue LED coupled to the epifluorescence path of the microscope. Light was delivered to the brain slice through a 0.80 NA 40× water immersion objective. Optical power densities ranged from 6 to 48 mW/mm^2. Recording sweeps with light presentations were repeated 20–120 times. Sweeps were collected at 20 s intervals using a light duration of 0.5–5 ms, but most of the data were acquired using 1–2 ms light pulse. Sweeps that did not exhibit a light-evoked EPSP were excluded from analysis. A minimum of 13 sweeps with an EPSP was required to include a cell in the analysis. To determine the receptors contributing to EPSPs, 10 µM NBQX disodium salt (AMPA receptor antagonist; catalog #HB0442, Hello Bio) and 50 µM D-AP5 (NMDA receptor antagonist; catalog #HB0225, Hello Bio) were used. Drugs were bath applied for at least 10 min before data were collected.

Short-term synaptic plasticity. To examine short-term plasticity at Y_1R^+ neuron synapses, channelrhodopsin-assisted circuit mapping was used, as detailed above. Because optogenetic activation of Y_1R^+ neurons could elicit feedforward inhibition by activating GABAergic neurons in the local IC, 5 µM gabazine (also called SR95531 hydrobromide, $GABA_A$ receptor antagonist; catalog #HB0901, Hello Bio) and 1 µM strychnine hydrochloride (glycine receptor antagonist; catalog #S8753, Sigma-Aldrich) were added to the bath. A total of five EPSPs were elicited using 20 Hz trains of 0.5–2 ms light pulses. For analysis, cursors were placed at the beginning and end of the EPSP to determine the peak amplitude of the first EPSP. The peak amplitude of the following EPSPs was determined using the foot-to-peak method in which the peak amplitude was measured relative to the most negative point attained following the peak of the preceding EPSP. Paired pulse ratios (PPRs) were defined by calculating the ratio of (average amplitude of $EPSP_n$) / (average amplitude of $EPSP_1$) (Kim and Alger, 2001). Sweeps that exhibited recurrent excitation were excluded from the analysis.

Recurrent excitation recordings. To enhance recurrent excitation in brain slices, 5 µM gabazine and 1 µM strychnine were included in the ACSF solution (Tu et al., 2005). Activation of excitatory inputs mediated by Y_1R^+ neurons was achieved by transfecting Y_1R^+ neurons with Chronos or ChroME and using brief flashes of blue light to activate Y_1R^+ inputs. After light presentation (0.5–5 ms), a large recurrent excitation was elicited causing the membrane to reach threshold and fire action potentials. After recording at least 20 sweeps in control condition, LP-NPY (500 nM; catalog #1176, Tocris Bioscience) was bath applied for ~10 min. After application of LP-NPY, the bath solution was returned to control ACSF, and washout responses were measured 10–30 min later. The number of action potentials was calculated in the control condition, during application of LP-NPY and washout. Action potentials were counted using a custom threshold-crossing algorithm in Igor Pro 9 software (WaveMetrics). Threshold was defined by eye for each cell. To measure the cumulative depolarization elicited, we calculated the area under the current-clamp depolarization trace (units of mV ms). To do this, data were first median filtered using a 4000 sample (80 ms) smoothing window to remove action potentials and isolate the underlying waveform of the depolarization. The area under the median-filtered depolarization relative to the baseline membrane potential was then calculated by trapezoidal integration (the 'area' function in Igor Pro).

To determine the effect of LP-NPY on recurrent excitatory currents in the local IC, experiments were performed in voltage clamp, and brief pulses of blue light were presented to elicit a long-lasting excitatory current. Only cells with a depolarizing current that lasted >40 ms were included in the analysis. To measure the cumulative amount of current elicited (i.e., the total charge passed in units of femtocoulombs), the area under the curve for voltage-clamp traces relative to baseline current was

calculated for control, LP-NPY, and washout using trapezoidal integration (the 'area' function in Igor Pro). To test whether responses were synaptically mediated, 10 μM NBQX and 50 μM D-AP5 were bath applied for at least 10 min, and additional responses were collected.

To determine the effect of LP-NPY on recurrent excitation, values of the action potential number and the area under the curve (i.e., the depolarization or excitatory current trace) were plotted in Igor Pro 9 (WaveMetrics). A custom algorithm was used to identify the most negative value during LP-NPY application. We then calculated the average across nine sweeps during baseline, LP-NPY application, and washout. Baseline and washout were defined relative to the most negative peak of the LP-NPY effect (represented as $t = 0$; see Figs. 8*E*,*F*, 9*E*). Baseline was calculated using the average value of action potentials or area under the curve across 760–920 s (12.6–15.3 min) before the LP-NPY peak effect. Washout was calculated 540–700 s (9–11.6 min) after the LP-NPY peak effect (see Figs. 8*D*–*F*, 9*E*, gray bars).

Statistics. Statistical analyses were performed in Igor Pro 9 (WaveMetrics), R software (version 4.1.0; https://www.r-project.org) and MATLAB (version R2021a; MathWorks). Data were analyzed using the estimation statistics approach (Bernard, 2019; Calin-Jageman and Cumming, 2019; Calin-Jageman, 2022), which has been previously detailed in a study from our lab (Rivera-Perez et al., 2021). Data comparisons are shown using Gardner–Altman estimation plots (two groups) or Cumming estimation plots (three or more groups), which use bootstrap sampling to calculate the distribution and 95% confidence intervals of expected differences between experimental groups or conditions. The design of these plots was heavily influenced by the DABEST package in R (Ho et al., 2019). Mean difference plots are shown with scatter plots (see Fig. 3*B*–*G*), whereas paired mean difference plots use parallel coordinate plots to connect measures from individual cells across experimental conditions (see Figs. 4*B*, 5*B*, 8*G*,*H*, 9*G*,*H*). Bias-corrected and accelerated 95% bootstrap confidence intervals were calculated using the 'boot' package in R using 10,000 resampling iterations. Gardner-Altman and Cumming estimation plots are provided to illustrate the spread of the data and the size of differences between experimental conditions but were not used for hypothesis testing.

Statistical hypothesis testing was performed using two approaches. For the comparison of the intrinsic physiology between adapting and sustained Y_1R^+ neurons (see Fig. 3) we used the "independence test", which is a nonparametric permutation test (Strasser and Weber, 1999), as implemented in the "coin" package in R (Hothorn et al., 2006, 2008). The significance level (α) was adjusted to account for the multiple comparisons using Bonferroni correction. Other comparisons were made using linear mixed models (LMM) analysis, which we implemented using the "lme4" and "lmerTest" packages in R (Bates et al., 2015). For most experiments, effects were considered significant when $p < 0.05$. Because the baseline area under the curve for the voltage-clamp and current-clamp experiments, as well as the action potential number, varied largely across cells, we calculated the log of the raw data before running LMM (see Figs. 8 and 9). Principal component analysis (PCA) was done in MATLAB using the "coeff" function. The *k*-means test was performed after PCA using the "kmeans" function in MATLAB. The optimal value of *k* (clusters) was defined as two using the elbow method (see Fig. 3, inset). The statistical test used for each experiment is described below (see Results).

Results

78.4% of glutamatergic neurons in the IC express *Npy1r* mRNA

To identify neurons that express the Y_1R, we used Y_1R-Cre x Ai14 mice to label Y_1R^+ neurons with the tdTomato fluorescent protein (Padilla et al., 2016). To validate that these mice selectively expressed tdTomato in Y_1R^+ neurons, we performed *in situ* hybridization using RNAScope with probes targeted to *Npy1r*, *Vglut2*, and *tdTomato*. Two males and one female mouse age P59 were used for the assay. Using design-based stereology, we found that 79.8% (3726 of 4668) of *tdTomato*$^+$ neurons colabeled with *Npy1r* (Fig. 1, Table 1).

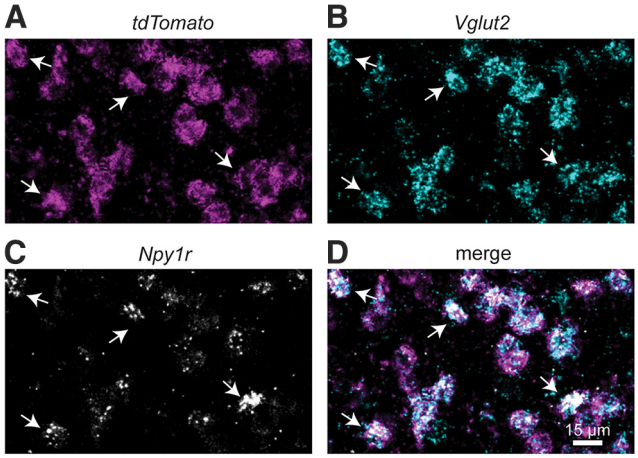

Figure 1. *tdTomato*$^+$ neurons express *Vglut2* and *Npy1r* mRNA. ***A–D***, High-magnification confocal images of a coronal IC section from a Y_1R-Cre x Ai14 mouse showing *tdTomato*$^+$ neurons (***A***, magenta) colabeled with *Vglut2* (***B***, cyan) and *Npy1r* (***C***, white; merge in ***D***). White arrows show examples of neurons that colabel. Scale bar, 15 μm.

In our previous study, we showed that only 1.1% of Y_1R^+ neurons colabeled with GAD67, a marker for GABAergic neurons, suggesting that most Y_1R^+ neurons are glutamatergic (Silveira et al., 2020). To confirm the neurotransmitter content of Y_1R^+ neurons, we used a probe targeted to *Vglut2*, which is a marker of glutamatergic cells in the IC (Ito et al., 2011). We found that 92% (4294 of 4668) of *tdTomato*$^+$ neurons express *Vglut2*. In very rare cases (0.4%), cells expressed *Npy1r* without the expression of *tdTomato* (15 of 3741 *Npy1r*-expressing neurons, Table 2). Regardless of the expression of tdTomato, 97.5% of *Npy1r*-expressing neurons expressed *Vglut2* (3647 of 3741). We then quantified the remaining glutamatergic cells (357 cells that did not express *tdTomato* and/or *Npy1r*) and found that *Npy1r*-expressing neurons represented 78.4% of glutamatergic cells in the IC (3647 of 4651; Table 2). This was a striking result as it shows that most IC glutamatergic neurons express *Npy1r*, suggesting that NPY signaling plays a major role in regulating excitatory neurons in the IC.

Previous studies described two subclasses of glutamatergic neurons in the IC, identified by the expression of VIP (Goyer et al., 2019) and CCK (Kreeger et al., 2021). To test whether Y_1R^+ neurons express *VIP* and/or *CCK*, we next performed *in situ* hybridization with probes targeted to *Npy1r*, *VIP*, and *CCK*. We found that many, but not all, *CCK* and *VIP* neurons expressed *Npy1r*. Interestingly, we also found that *VIP* and *CCK* expression could overlap, with many *VIP* neurons expressing *CCK* but *VIP*-expressing neurons representing only a subset of *CCK* neurons (Fig. 2, blue arrow indicates VIP^+CCK^+ Y_1R^-, white arrow indicates $VIP^-CCK^+Y_1R^+$, magenta arrow indicates $VIP^+CCK^+Y_1R^+$).

Y_1R^+ neurons exhibit heterogenous intrinsic physiology

Neurons in the IC exhibit diverse firing patterns, being broadly classified as sustained or adapting neurons (Peruzzi et al., 2000; Goyer et al., 2019; Silveira et al., 2020). By targeting whole-cell current-clamp recordings to Y_1R^+ neurons in acute brain slices from Y_1R-Cre x Ai14 mice, we previously showed that Y_1R^+ neurons exhibit either sustained or adapting firing patterns in response to depolarizing current steps (Silveira et al., 2020). Here, we expanded the recordings ($n = 38$ cells previously reported in Silveira et al., 2020 plus an additional $n = 55$ cells from this study). We found that Y_1R^+ neurons with sustained or

Table 1. tdTomato$^+$ (tdT$^+$) neurons are glutamatergic and express Y_1R

Mouse	Slice	*tdT*$^+$	*tdT*$^+$ *Vglut2*$^+$	% *tdT*$^+$*Vglut2*$^+$/*tdT*$^+$	*tdT*$^+$ *Npy1r*$^+$	% *tdT*$^+$*Npy1r*$^+$/*tdT*$^+$
Female P59	Caudal	278	254	91.4	180	64.7
	Medial	371	334	90.0	264	71.2
	Rostral	432	403	93.3	344	79.6
Male P59	Caudal	464	426	91.8	331	71.3
	Medial	421	390	92.6	319	75.8
	Rostral	260	235	90.4	195	75.0
Male P59	Caudal	522	478	91.6	444	85.1
	Medial	1120	1026	91.6	964	86.1
	Rostral	800	748	93.5	685	85.6
Total		4668	4294	92.0	3726	79.8

Table 2. Y_1R^+ Neurons represent 78.4% of IC glutamatergic cells

Mouse	Slice	*Npy1r*$^+$	*Npy1r*$^+$ *Vglut2*$^+$	% *Npy1r*$^+$ *Vglut2*$^+$ /*Npy1r*$^+$	*Npy1r*$^+$ *tdT*$^-$	*Vglut2*$^+$	% *Npy1r*$^+$ *Vglut2*$^+$/*Vglut2*$^+$
Female P59	Caudal	181	172	95.0	1	283	60.8
	Medial	265	249	94.0	1	375	66.4
	Rostral	348	340	97.7	4	418	81.3
Male P59	Caudal	336	329	97.9	5	477	69.0
	Medial	321	317	98.8	2	425	74.6
	Rostral	195	189	96.9	0	262	72.1
Male P59	Caudal	446	435	97.5	2	522	83.3
	Medial	964	942	97.7	0	1092	86.3
	Rostral	685	674	98.4	0	797	84.6
Total		3741	3647	97.5	15	4651	78.4

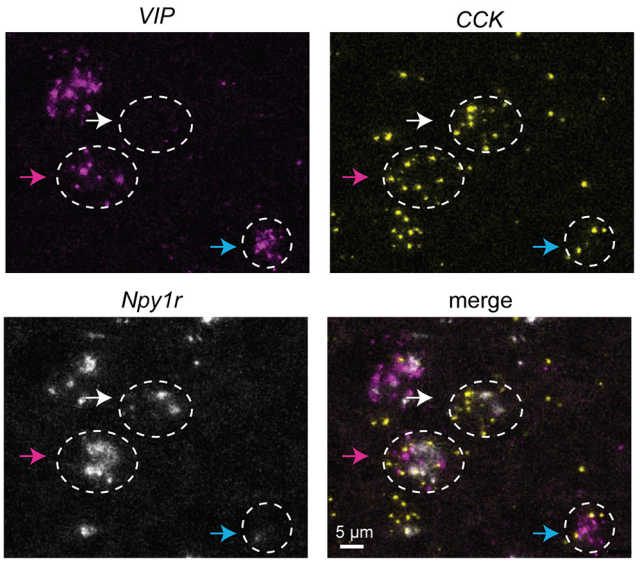

Figure 2. Y_1R^+ neurons can express *VIP* and/or *CCK*. High-magnification confocal images of a coronal IC section showing *VIP* (magenta), *CCK* (yellow), and *Npy1r* (white) expression. Arrows indicate examples of cells that are *VIP*$^+$*CCK*$^+$*Y*$_1$*R*$^-$ (blue arrows); *VIP*$^-$*CCK*$^+$*Y*$_1$*R*$^+$ (white arrows); and *VIP*$^+$*CCK*$^+$*Y*$_1$*R*$^+$ (magenta arrows). Dotted circles represent individual neurons. Scale bar, 5 μm.

adapting firing patterns exhibited heterogeneous intrinsic properties. Neurons were classified as sustained or adapting according to their spike frequency adaption ratio (SFA). Neurons with an SFA >2 were classified as adapting, and neurons with SFA <2 were classified as sustained (Peruzzi et al., 2000). Most neurons had a sustained firing pattern in response to a depolarizing current step (60 of 93 neurons had an SFA ratio <2, and 33 of 93 neurons had an SFA ratio >2; Fig. 3*A*,*B*; SFA ratio with five spikes comparing sustained vs adapting neurons, unpaired independence test, $Z = 6.30$, $p <$ 1e-04; Bonferroni-corrected $\alpha = 0.0083$). The membrane time constant was calculated by hyperpolarizing the cell membrane potential by 2–6 mV in a series of sweeps, fitting an exponential function to each response, and obtaining the median τ. Sustained Y_1R^+ neurons had a slower membrane time constant (15.39 ± 4.90 ms) compared with adapting neurons (8.40 ± 4.90 ms; independence test, $Z = -4.44$, $p <$ 1e-04; Bonferroni-corrected $\alpha = 0.0083$; Fig. 3*C*). In response to hyperpolarizing current injections, adapting Y_1R^+ neurons exhibited a more prominent depolarizing sag, suggesting a higher expression of HCN channels (steady state/peak, measured from current steps that elicited peak hyperpolarization of −91.0 ± 0.9 mV; voltage sag ratio of 0.74 ± 0.19 for adapting neurons, and 0.88 ± 0.14 for sustained neurons; independence test, $Z = -3.56$, $p <$ 1e-04; Bonferroni-corrected $\alpha = 0.0083$; Fig. 3*D*). The minimal amount of current required to elicit an action potential (rheobase) was lower for sustained neurons (56.18 ± 37.63 pA) compared with adapting neurons (77.94 ± 47.23 pA; independence test, $Z = 2.37$, $p = 0.01$; Bonferroni-corrected $\alpha = 0.0083$; Fig. 3*E*). Resting membrane potential was measured shortly after whole-cell recording mode was achieved and was similar between adapting and sustained neurons (−67.9 ± 6.5 mV for adapting neurons and −69.3 ± 6.6 mV for sustained neurons, independence test, Z = 0.96, $p =$ 0.33; Bonferroni-corrected $\alpha = 0.0083$; Fig. 3*F*). Finally, sustained neurons exhibited a higher input resistance (266.8 ± 99.5 MΩ, measured at the peak of the hyperpolarizing response) compared with adapting neurons (167.9 ± 74.7 MΩ, independence test, $Z = -10.57$, $p <$ 1e-04; Bonferroni-corrected $\alpha =$ 0.0083; Fig. 3*G*).

We next performed PCA to test whether Y_1R^+ neurons can be divided into multiple cell types based on intrinsic physiology. The PCA was performed using the following parameters: membrane time constant, voltage sag ratios, rheobase, resting membrane potential, input resistance, and SFA ratio. The results showed that the first principal component explained 92.28% of the variability in the data, and the second component explained 7.14% of the variability. Despite largely different intrinsic

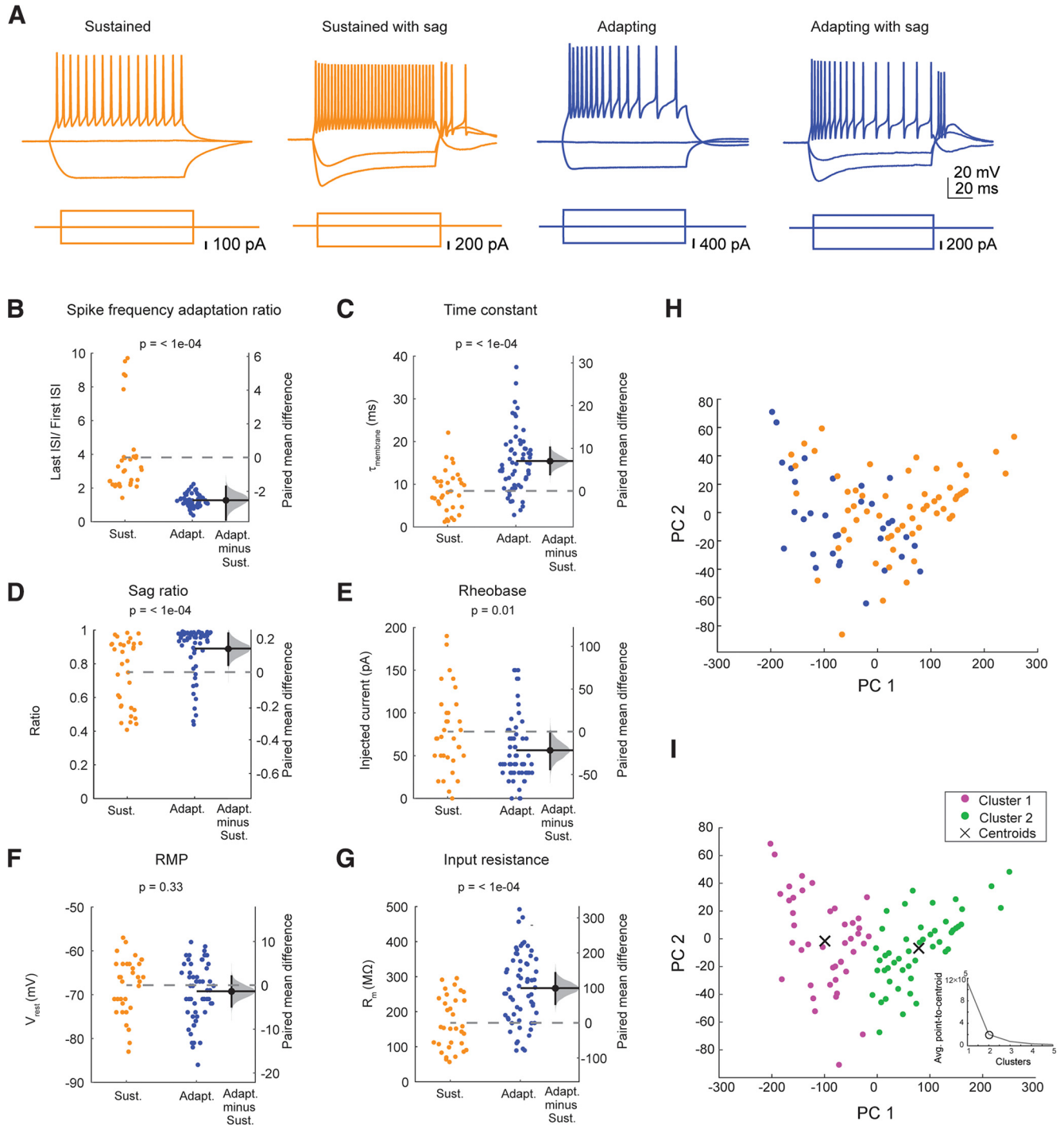

Figure 3. Y_1R^+ neurons exhibit sustained or adapting firing patterns. ***A***, Y_1R^+ neurons exhibited different combinations of firing patterns and hyperpolarization-induced sag. Orange indicates neurons with a sustained firing pattern with or without voltage-dependent sag, and blue indicates neurons with an adapting firing pattern with or without voltage-dependent sag. ***B–G***, Sustained and adapting neurons exhibited heterogenous intrinsic physiological properties. ***B***, Spike frequency adaptation ratio. ***C***, Membrane time constant. ***D***, Voltage-dependent sag ratio. ***E***, Rheobase. ***F***, Resting membrane potential. ***G***, Input resistance. Dashed gray lines represent the level of zero difference in the mean difference plots. ***H***, Principal components analysis showed that the distributions of adapting (blue) and sustained (orange) neurons overlapped. ***I***, Separation of Y_1R^+ neurons into two clusters using *k*-means cluster analysis yielded clusters that did not match those predicted from sustained and adapting firing patterns (compare ***H*** and ***I***). Magenta and green dots represent the two different clusters; 69.7% of adapting neurons fell into cluster 1, and 65.0% of sustained neurons fell into cluster 2. Inset, bottom right, The number of clusters used for analysis was defined using the elbow analysis, which showed that the addition of a third cluster did little to improve the separation between cluster centroids.

physiology, the PCA analysis did not separate Y_1R^+ neurons with adapting or sustained firing patterns into nonoverlapping clusters (Fig. 3*H*). To probe this quantitatively, we used *k*-means cluster analysis. With *k*-means cluster analysis set to identify two clusters, we found that the majority of adapting neurons (69.70%) were part of cluster 1 and most sustained neurons (65%) fell into cluster 2 (Fig. 3*I*). These data suggest that although individual intrinsic properties differ between adapting and sustained neurons at the population level, these differences do not completely separate Y_1R^+ neurons into two

different groups. This is likely because of the variability in intrinsic physiology within each neuron group, which often overlapped between sustained and adapting neurons. These results suggest that IC Y_1R^+ neurons encompass two or more classes of glutamatergic neurons and provide additional support for the observation that IC neurons are difficult to classify based on physiology alone (Reetz and Ehret, 1999; Peruzzi et al., 2000; Sivaramakrishnan and Oliver, 2001; Ono et al., 2005; Palmer et al., 2013; Goyer et al., 2019; Kreeger et al., 2021).

Y_1R^+ neurons form interconnected networks in the local IC

The IC is rich in local circuits, with anatomic reports indicating that most neurons have local axon collaterals (Oliver et al., 1991; Ito et al., 2016). However, very few studies have examined the functional organization of local circuits in the IC, and it is unknown how different populations of neurons contribute to IC local circuits. To investigate how Y_1R^+ neurons contribute to local circuits, we used viral transfections to express the excitatory opsin Chronos-GFP (Klapoetke et al., 2014) in Y_1R^+ neurons in one side of the IC, and then we targeted our recordings to either Y_1R^+ neurons or Y_1R^- neurons in the transfected side of the IC. As most glutamatergic IC neurons express Y_1R, and glutamatergic neurons represent ~75% of neurons in the IC (Oliver et al., 1994; Beebe et al., 2016), we estimate that there is an ~77% chance that Y_1R^- neurons are GABAergic neurons. This estimate is based on previous reports that GABAergic neurons represent ~25% of IC neurons and our *in situ* hybridization result showing that *tdTomato* is expressed by 92.5% of glutamatergic neurons in the IC, 25% / (25% + 7.5%) = 77%. However, as no GABAergic marker was used to identify these cells, we refer to these neurons as Y_1R^- neurons.

First, we targeted recordings to Y_1R^+ neurons that were not transfected with Chronos in acute brain slices. We found that activation of Y_1R^+ terminals with brief pulses of blue light (0.5–5 ms) elicited EPSPs in most Y_1R^+ neurons (Fig. 4*A–C*; 14 of 16 neurons recorded). Neurons in the IC can express NMDA receptors that are relatively insensitive to Mg^{2+} block and therefore readily conduct current at resting membrane potential (Wu et al., 2004; Goyer et al., 2019; Drotos et al., 2023). To test whether such NMDA receptors are present at Y_1R^+ synapses onto Y_1R^+ neurons, we bath applied 10 μM NBQX, which is an AMPA receptor antagonist. In the presence of 10 μM NBQX, the light-evoked EPSP was incompletely blocked in 10 of 14 cells, suggesting the presence of an NMDA component [amplitude in control condition, 4.6 mV ± 3.0 mV; amplitude in NBQX, 0.6 mV ± 0.5 mV; LMM, $\beta = -4.01$, 95% CI (−5.33, −2.69), $p = 1.36e\text{-}05$, n = 14. Fig. 4*B,C*]. The EPSPs were completely abolished when 50 μM D-AP5, an NMDA receptor antagonist, was added to the ACSF containing NBQX [LMM, $\beta = -2.72$, 95% CI (−6.21, −2.94), $p = 1.88e\text{-}05$, $n = 4$; Fig. 4*B,C*).

Next, we targeted our recordings to Y_1R^- neurons that were identified by a lack of tdTomato expression. We found that presentation of 1–2 ms light pulses elicited EPSPs in six of six cells tested. Interestingly, after application of 10 μM NBQX, only one cell had an incompletely blocked EPSP, suggesting the presence of an NMDA component [Fig. 5*A–C*, amplitude in control condition, 2.8 mV ± 1.0 mV; amplitude in NBQX, 0.1 mV ± 0.3 mV; LMM, $\beta = -4.01$, 95% CI (−3.51, −1.93), $p = 5.23e\text{-}05$, $n = 6$]. Addition of 50 μM D-AP5 completely abolished the EPSP. Because the NMDA component was present in only one cell, we did not run statistical analysis on these data, but we show the raw data in Figure 5*C*. Together, these data suggest that Y_1R^+ neurons form interconnected neuronal circuits in the local IC by synapsing onto other Y_1R^+ neurons as well as Y_1R^- neurons. We cannot rule out the possibility that these interconnections are formed by a small portion of Y_1R^+ neurons branching profusely. However, given that most IC neurons have local axon collaterals, it is likely that many or most Y_1R^+ neurons contribute to excitatory connections within local IC circuits.

Y_1Rs synapses have modest short-term synaptic plasticity

To investigate whether inputs mediated by Y_1R^+ neurons exhibit short-term synaptic plasticity, we recorded from 10 Y_1R^+ neurons and 8 Y_1R^- neurons while presenting blue light pulses to activate Y_1R^+ inputs. For most recordings we used viral transfections to express a soma-targeted variant of the excitatory opsin ChroME in Y_1R^+ neurons (6 of 10 Y_1R^+ neuron recordings, 8 of 8 Y_1R^- neuron recordings; Mardinly et al., 2018). Soma-targeted ChroME allowed us to study synaptic events generated by eliciting action potentials in the cell body providing a more physiological condition for short-term synaptic plasticity experiments. In 4 of the 10 recordings from Y_1R^+ neurons, Chronos was expressed instead of soma-targeted ChroME. In these recordings, we cannot rule out the possibility that vesicular release was achieved by direct depolarization of synaptic terminals (Petreanu et al., 2009). Because no difference was observed between these approaches, the data were combined. Because our data suggest that optogenetic activation of Y_1R^+ neurons can excite GABAergic neurons in the local IC, possibly eliciting feedforward inhibition, 5 μM gabazine and 1 μM strychnine hydrochloride were included in the bath ACSF to isolate EPSPs.

We used 20 Hz train stimulation to elicit EPSPs (Fig. 6) and obtained the PPR by dividing the average peak amplitude of the second, third, or fourth EPSP over the average peak amplitude of the first EPSP (see above, Materials and Methods). Interestingly, we saw little short-term synaptic plasticity when recording either from Y_1R^+ or Y_1R^- neurons. The PPR values when recording from Y_1R^+ neurons were as follows: $EPSP_2/EPSP_1 = 0.90 \pm 0.19$, $EPSP_3/EPSP_1 = 0.83 \pm 0.17$, $EPSP_4/EPSP_1 = 0.86 \pm 0.27$, and $EPSP_5/EPSP_1 = 0.84 \pm 0.21$ (mean ± SD). PPR values were not significantly different from 1 (one-sample Student's *t* test comparing data to mean = 1, 1 vs $EPSP_2/EPSP_1$, $p = 0.13$; 1 vs $EPSP_3/EPSP_1$, $p = 0.013$; 1 vs $EPSP_4/EPSP_1$, $p = 0.16$; 1 vs $EPSP_5/EPSP_1$, $p = 0.04$; Bonferroni-corrected $\alpha = 0.0125$, $n = 10$). The PPR values determined from Y_1R^- neurons were as follows: $EPSP_2/EPSP_1 = 1.07 \pm 0.18$, $EPSP_3/EPSP_1 = 1.00 \pm 0.20$, $EPSP_4/EPSP_1 = 0.96 \pm 0.19$, and $EPSP_5/EPSP_1 = 0.90 \pm 0.18$. PPR values in Y_1R^- neurons were not significantly different from 1 (one-sample Student's *t* test comparing data to mean = 1, 1 vs $EPSP_2/EPSP_1$, $p = 0.29$; 1 vs $EPSP_3/EPSP_1$, $p = 0.96$; 1 vs $EPSP_4/EPSP_1$, $p = 0.64$; 1 vs $EPSP_5/EPSP_1$, $p = 0.19$; Bonferroni-corrected $\alpha = 0.0125$, $n = 8$). These data suggest that Y_1R^+ synapses in local IC circuits possess mechanisms that maintain synaptic strength during periods of repeated activity, thereby resulting in little short-term synaptic plasticity overall.

NPY decreases recurrent excitation in the IC

NPY is one of the most abundant neuropeptides in the brain and has been shown to modulate neuronal circuits in many brain regions (Colmers and Bleakman, 1994; Gutman et al., 2008; van den Pol et al., 2009; van den Pol, 2012). In the hippocampus, for example, NPY decreases recurrent excitation (Tu et al., 2005). Our data show that most glutamatergic neurons in the IC express Y_1R and that Y_1R^+ neurons are interconnected with other Y_1R^+ and Y_1R^- neurons in local IC circuits. This raises the hypothesis

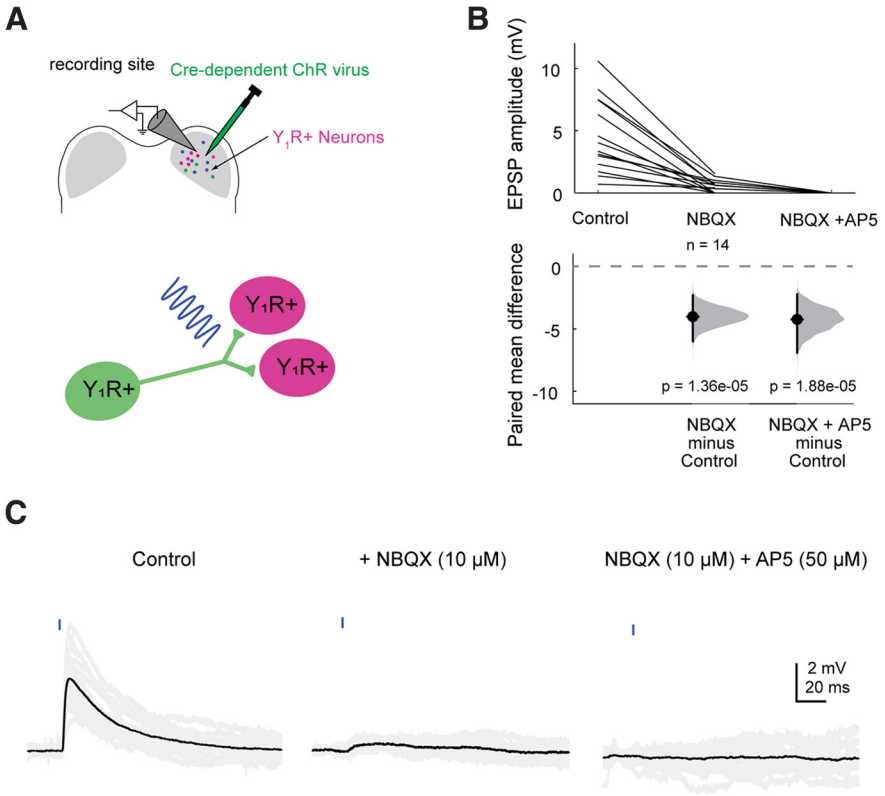

Figure 4. Y_1R^+ neurons synapse onto other Y_1R^+ neurons. ***A***, Diagram representing the experimental setup. A Cre-dependent AAV was injected into one side of the IC to drive Chronos expression in Y_1R^+ neurons. After allowing 2–4 weeks for opsin expression, recordings were targeted to Y_1R^+ neurons in the transfected side of the IC. A brief pulse of blue light was used to activate Y_1R^+ terminals. ***B***, Light pulses elicited EPSPs of varying amplitudes. These EPSPs were blocked by 10 μM NBQX in 10 of 14 cells tested. The remaining EPSPs were abolished after application of 50 μM D-AP5. The dashed gray line indicates the level of zero difference in the paired mean difference plot. ***C***, Example traces of optogenetically evoked EPSPs recorded from a Y_1R^+ neuron in the IC ipsilateral to the injection site. Black traces represent average responses, and gray traces represent individual sweeps.

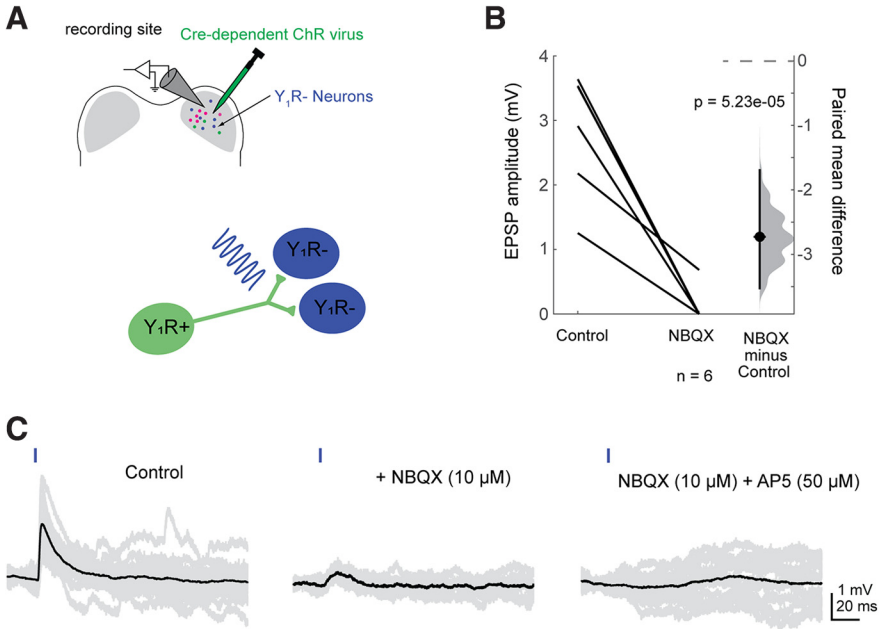

Figure 5. Y_1R^+ neurons synapse onto other Y_1R^- neurons. ***A***, Diagram representing the experimental setup. A Cre-dependent AAV was injected into the right IC to drive Chronos expression in Y_1R^+ neurons. After allowing 2–4 weeks for virus expression, recordings were targeted to Y_1R^- neurons in the transfected side of the IC. A brief pulse of blue light was used to activate Y_1R^+ terminals. ***B***, Light pulses elicited EPSPs of varying amplitudes. Application of 10 μM NBQX abolished EPSPs in five of six cells tested. In the sixth cell, the remaining EPSP was abolished with application of 50 μM D-AP5 (data not shown). ***C***, Example traces of optogenetically evoked EPSPs recorded from a Y_1R^- neuron in the IC ipsilateral to the injection site. EPSPs are from the only Y_1R^- neuron that exhibited an NMDA component in its response. Black traces represent average responses, and gray traces represent individual sweeps.

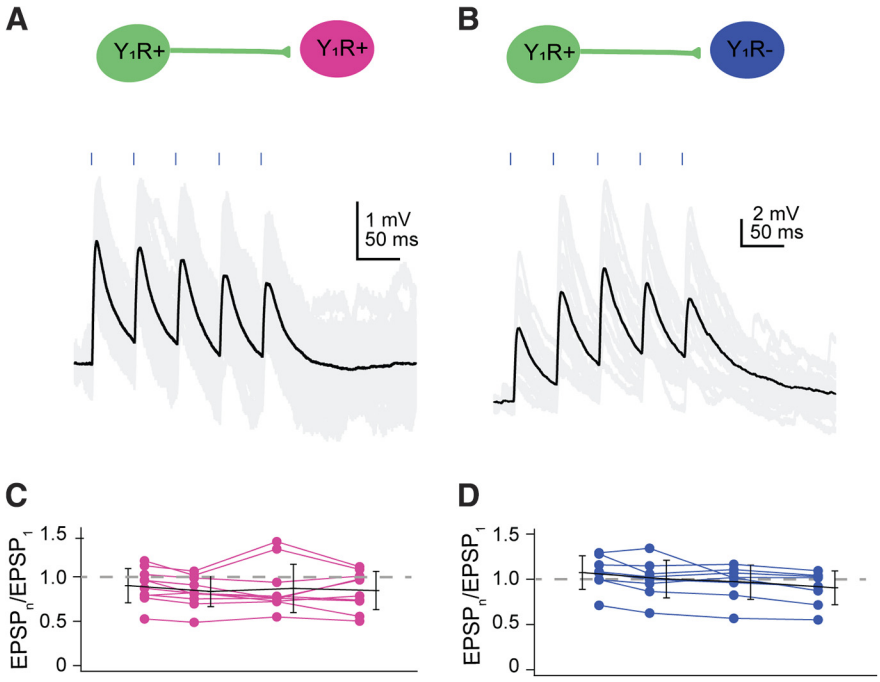

Figure 6. Y_1R^+ synapses exhibit moderate short-term synaptic plasticity. ***A***, ***B***, Example traces from a Y_1R^+ neuron (***A***) and a Y_1R^- neuron (***B***) showing EPSPs evoked by 20 Hz trains of light pulses. Black traces represent average responses and gray traces represent individual sweeps. ***C***, ***D***, Plots of the PPRs for Y_1R^+ synapses onto Y_1R^+ neurons (***C***) and Y_1R^- neurons (***D***) reveal little short-term plasticity. Each dot represents (average $EPSP_n$) / (average $EPSP_1$) for an individual cell. Solid black line represents the SD. Dashed gray lines indicate PPR of one.

that NPY signaling regulates the excitability of local circuits in the IC. To test this hypothesis, we used a combination of pharmacology and optogenetics to generate recurrent excitation *in vitro*. For that, Y_1R-Cre x Ai14 mice were injected with viruses to selectively express soma-targeted ChroME (10 of 11 cells) or Chronos (1 of 11 cells) in Y_1R^+ neurons. To increase the probability of recurrent excitation during slice recordings, we included 5 μM gabazine ($GABA_A$ receptor antagonist) and 1 μM strychnine (glycinergic receptor antagonist) in the ACSF (Tu et al., 2005). When Y_1R^+ neurons were activated with a brief flash of blue light, prolonged trains of excitatory events, consistent with recurrent excitation, were observed in both Y_1R^+ and Y_1R^- neurons (Fig. 7).

First, we targeted whole-cell current-clamp recordings to two Y_1R^+ neurons and three Y_1R^- neurons. A brief presentation of blue light (0.5–5 ms) elicited recurrent excitation that elicited trains of action potentials in the recorded neurons (Fig. 8*A*). Bath application of 500 nM LP-NPY, a Y_1R agonist, decreased recurrent excitation, decreasing the number of action potentials elicited by the blue light pulse [LMM, $\beta = -0.43$, 95% CI (-0.66, -0.19), $p = 0.007$, $n = 5$; Fig. 8*B*,*E*,*G*]. After a 10–20 min washout in control ACSF, the number of action potentials elicited by recurrent excitation was similar to that of control [LMM, $\beta = -0.07$, 95% CI (-0.30, 0.16), $p = 0.57$, n = 5; Fig. 8*C*,*E*,*G*]. In four of five cells we applied NBQX and D-AP5 to verify that the recurrent excitation was synaptically driven (Fig. 8*D*). In only one cell (a Y_1R^+ neuron) a brief EPSP persisted in the presence of synaptic blockers (amplitude, 13.5 ± 0.3 mV; half-width, 13.8 ± 0.6 ms; data not shown). However, as it was a brief EPSP, it could not explain the long-lasting recurrent excitation observed in this experiment. We previously showed that NPY can directly hyperpolarize the membrane potential of Y_1R^+ neurons (Silveira et al., 2020); however, here we did not see a correlation between resting membrane potential and the number of action potentials elicited by activation of Y_1R^+ neurons (data not shown; linear correlation test; cell 1, Y_1R^+, $r^2 = -0.071$, $p = 0.004$; cell 2, Y_1R^+, $r^2 = 0.085$, $p = 0.005$; cell 3, Y_1R^-, $r^2 = -0.001$, $p = 0.690$; cell 4, Y_1R^-, $r^2 = -0.018$, $p = 0.181$; cell 5, Y_1R^-, $r^2 = -0.074$, $p = 0.005$).

To measure the cumulative depolarization elicited by recurrent excitation, we next calculated the area under the depolarizing trace relative to the baseline membrane potential. As detailed (see above, Materials and Methods), we used a median filter to isolate the steady depolarization underlying the train of action potentials before determining the area under the depolarizing trace using trapezoidal integration. Application of LP-NPY led to a decrease in the area under the curve [LMM, $\beta = -0.44$, 95% CI (-0.65, -0.23), $p = 0.003$, $n = 5$], and the effect was reversed during washout [LMM, $\beta = -0.005$, 95% CI (-0.21, 0.20), $p = 0.84$, $n = 5$; Fig. 8*F*,*H*]. Graphs in Figure 8, *E* and *F*, represent the changes in action potential number and area under the curve across the duration of each recording.

Next, we performed voltage-clamp experiments to investigate how NPY signaling shapes recurrent excitatory currents in the local IC. In recordings from four Y_1R^+ neurons and two Y_1R^- neurons, we used optogenetics to activate Y_1R^+ neurons and saw long-lasting excitatory currents in the recorded neurons (Fig. 9*A*–*C*). Application of LP-NPY decreased the recurrent excitatory current, as measured by the area under the evoked inward current relative to the baseline current [LMM, $\beta = -0.25$, 95% CI (-0.45, -0.06), $p = 0.03$, $n = 6$; Fig. 9*E*,*F*]. Washout responses were obtained in four cells, showing a reversal of the LP-NPY effect [LMM, $\beta = 0.14$, 95% CI (-0.08, 0.37), $p = 0.25$, $n = 4$]. In these four cells, we next applied NBQX (10 μM) + D-AP5 (50 μM) to verify that excitatory responses were synaptically driven (Fig. 9*D*). The response was completely abolished in three of four cells tested (data not shown). In the fourth cell, the half-width of the remaining event was very brief (0.58 ± 0.01 ms), and therefore it could not explain the prolonged excitatory currents observed in that cell. In one additional cell, the

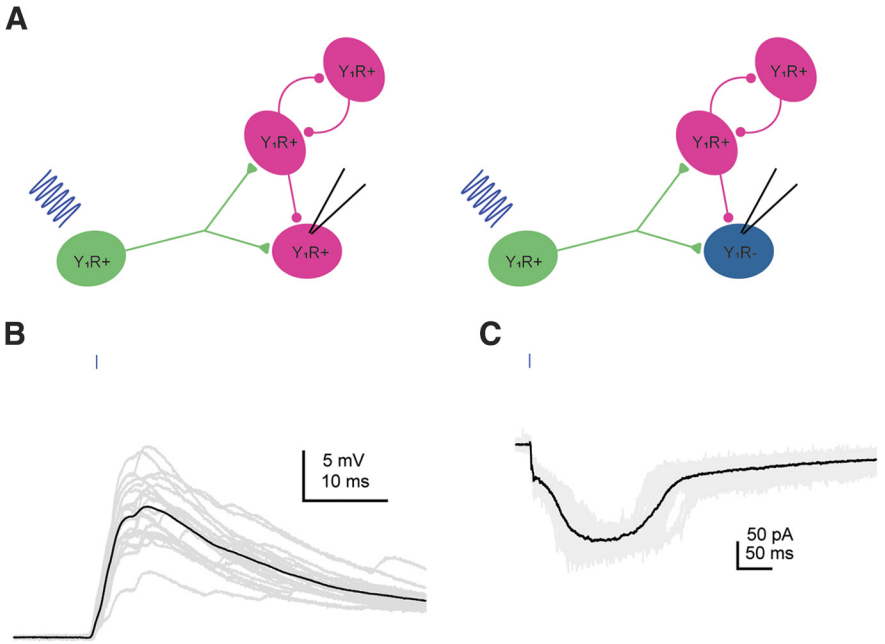

Figure 7. Activation of Y_1R^+ neurons elicits recurrent excitation in the IC. ***A***, Diagram showing experimental design. Viruses expressing Chronos or ChroME were used to transfect Y_1R^+ neurons. In the presence of inhibitory synaptic blockers (5 μM gabazine and 1 μM strychnine), optogenetic activation of Y_1R^+ neurons elicited prolonged periods of recurrent excitation. Recordings were targeted both to Y_1R^+ and Y_1R^- neurons. ***B***, ***C***, Examples of recurrent excitation from a current-clamp recording (***B***) and a voltage-clamp recording (***C***). Example trace in ***B*** is from a Y_1R^+ neuron, and example trace in ***C*** is from a Y_1R^- neuron.

recurrent excitation increased throughout the recording session, and therefore it was excluded from the final analysis. Together, these data suggest that NPY signaling plays an important role in regulating excitatory networks in local IC circuits.

Discussion

Here, we showed that nearly 80% of glutamatergic neurons in the IC express mRNA encoding the NPY Y_1R. Using targeted recordings and optogenetics, we found that Y_1R^+ neurons provide excitatory input to most other Y_1R^+ and Y_1R^- neurons in the IC and therefore form interconnected networks within local IC circuits. Excitatory synapses between Y_1R^+ neurons and other IC neurons exhibited modest short-term synaptic plasticity, suggesting a balance between synaptic facilitation and depression that results in a stable strength of excitatory synaptic signaling in local circuits. Furthermore, we found that NPY shaped local excitation in the IC by inhibiting recurrent excitatory circuits. Thus, our data provide functional evidence that IC glutamatergic neurons form densely interconnected local circuits and indicate that NPY is a major modulator of local circuit operations in the auditory midbrain.

Most excitatory neurons in the IC express the NPY Y_1R

Neurons that express the Y_1R are widely distributed in the brain (Eva et al., 2006). Y_1Rs are mainly postsynaptic (Wahlestedt et al., 1986; Kopp et al., 2002; Fu et al., 2004), but can also be found at presynaptic sites (Dumont et al., 1998; Glass et al., 2002). The neurotransmitter content of Y_1R^+ neurons vary across brain regions. In the amygdala and hypothalamus, Y_1R can be expressed by GABAergic and glutamatergic neurons (Roseberry et al., 2004; Rostkowski et al., 2009; Wittmann et al., 2013). In the prefrontal cortex (Vollmer et al., 2016) and spinal cord (Nelson et al., 2019), most Y_1R^+ neurons are glutamatergic. Strikingly, in the IC, which is well known for its neuronal diversity (Peruzzi et al., 2000; Palmer et al., 2013; Beebe et al., 2016), Y_1R^+ neurons almost completely overlapped with *Vglut2*$^+$ neurons and very rarely colabeled with GAD67 (Silveira et al., 2020).

Because Y_1R^+ neurons represent most of the glutamatergic neurons in the IC, the Y_1R^+ population likely includes neurons with disk-shaped and stellate morphologies. Consistent with this, we found that Y_1R^+ neurons could express *VIP*, a marker for a class of stellate neurons (Goyer et al., 2019), and/or *CCK*, a marker for a class of disk-shaped neurons (Kreeger et al., 2021). Interestingly, we found that *VIP* and *CCK* mRNA were occasionally present in the same neurons. This was unexpected because of the different morphologies previously reported for VIP and CCK neurons. However, there are at least two reasonable explanations for this. First, CCK neurons were identified in gerbils (Kreeger et al., 2021), raising the possibility of species differences. Second, CCK neurons were identified using a viral approach, which labeled ~75% of neurons expressing *CCK* mRNA (Kreeger et al., 2021). Thus, it is likely that the *VIP*$^+$ *CCK*$^+$ neurons observed here represent a group of CCK-expressing neurons that was not labeled by the viral strategy used in the Kreeger study.

The fact that NPY is expressed in approximately one-third of GABAergic IC neurons (Silveira et al., 2020), whereas Y_1R is expressed in most glutamatergic IC neurons represents a major step toward understanding the functional organization of neuronal circuits in the IC. As our results indicate that Y_1R^+ neurons encompass multiple classes of IC glutamatergic neurons, it will be important to determine whether activation of Y_1Rs by NPY signaling inhibits different classes of IC excitatory neurons in subtly different ways or whether NPY signaling broadly and equally dampens all local excitatory activity in the IC.

Y_1R^+ neurons form interconnected local circuits in the IC

Anatomical studies suggest that most IC neurons have local axon collaterals (Oliver et al., 1991; Saldaña and Merchán, 2005; Chen et al., 2018). Previous studies using laser scanning glutamate

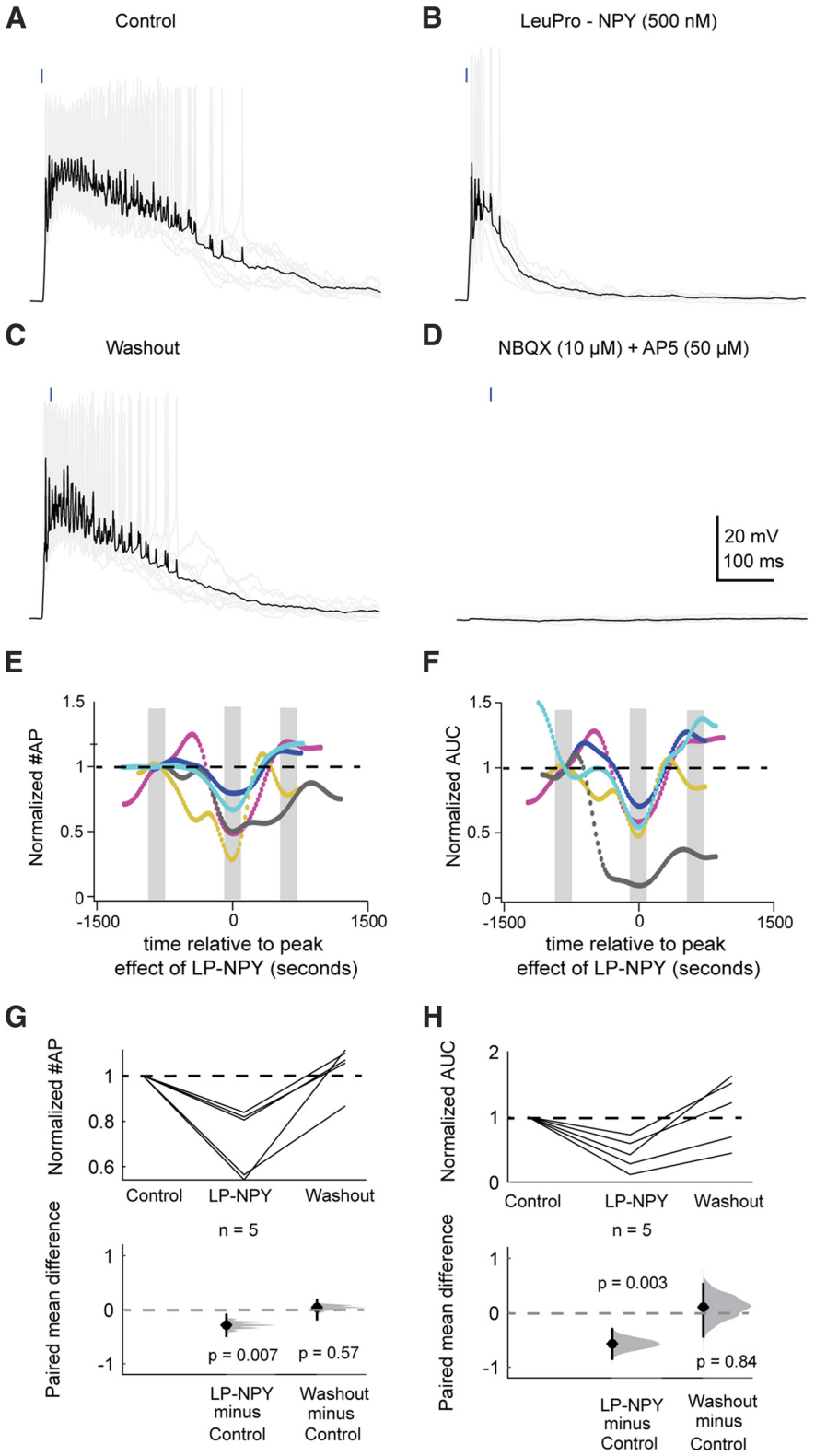

Figure 8. Application of LP-NPY decreases action potentials elicited by recurrent excitation. ***A–D***, In a recording from a Y_1R^+ neuron, activation of other Y_1R^+ neurons using a brief light pulse (represented by blue rectangles) elicited recurrent excitation that resulted in action potentials (***A***). Bath application of the Y_1R agonist, LP-NPY (500 nM), decreased recurrent excitation resulting in a decrease in action potential number (***B***). This effect was reversed during washout (***C***). Recurrent excitation was completely abolished by application of 10 μM NBQX and 50 μM D-AP5 (***D***). ***E***, Graph shows normalized action potential number across the total duration of the recordings. Data are plotted relative to the most negative point during LP-NPY application (time = 0). Gray bars indicate the data points that were analyzed for baseline, LP-NPY application, and washout. Black dashed line represents the level of one. Each color represents one individual cell, and each dot represents a single trial. Trails were run at 20 s intervals. ***F***, Graph showing normalized area under the curve (i.e., area under the median-filtered depolarization relative to the baseline membrane potential) across the recorded cells. Colors correspond to cells in ***E***. Data are plotted relative to the most negative point during LP-NPY application (time = 0). Gray bars represent the data points that were analyzed for baseline, LP-NPY application, and washout. Black dashed line represents the level of one. ***G***, ***H***, Application of LP-NPY decreased the

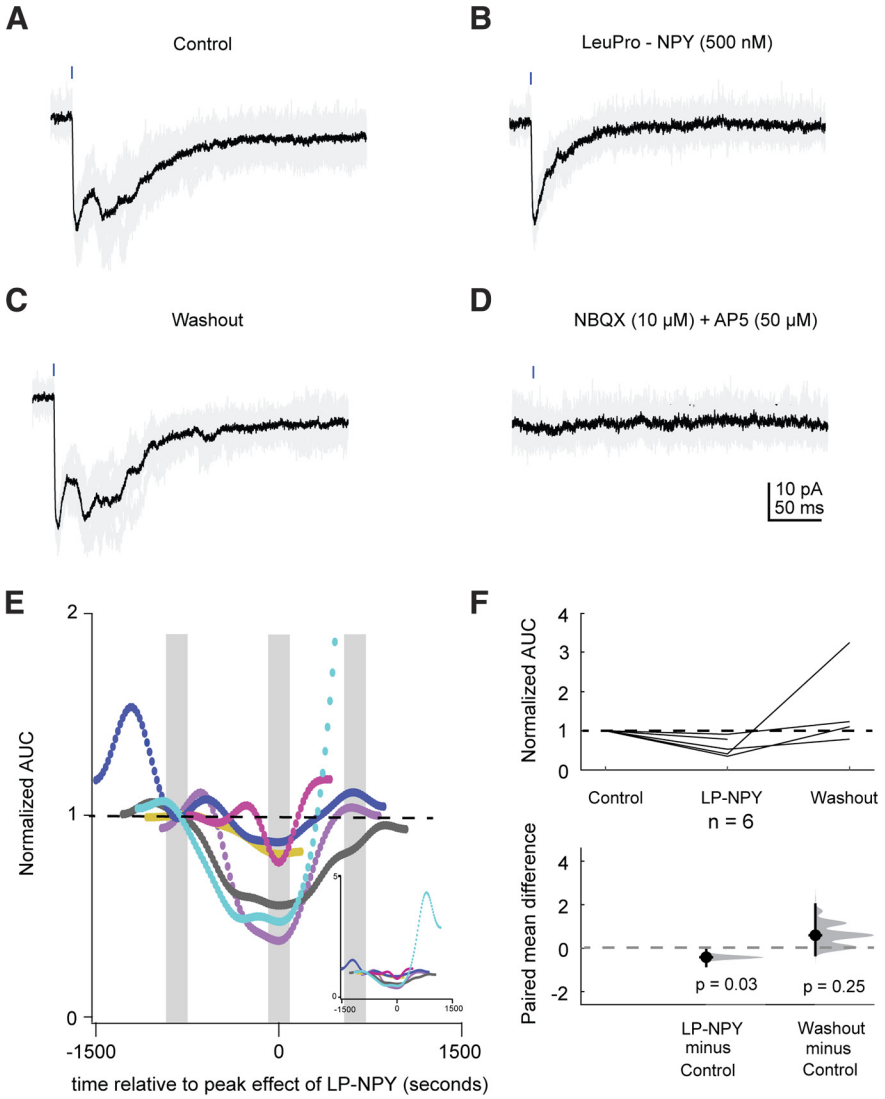

Figure 9. Application of LP-NPY decreases recurrent excitatory current. ***A–D***, Activation of Y_1R^+ neurons by a brief light pulse (represented by blue rectangles) elicited recurrent excitatory currents in an example recording from a Y_1R^+ neuron (***A***). Bath application of LP-NPY (500 nM) decreased recurrent excitation (***B***). This effect was reversed during washout (***C***). The recurrent excitatory current was abolished by 10 μM NBQX and 50 μM D-AP5 (***D***). ***E***, Graph showing normalized area under the curve (i.e., area under the evoked inward current relative to baseline current) across 6 cells. Each dot represents one trial, with trial responses collected at 20 s intervals. Data are plotted relative to the most negative point during LP-NPY application (time = 0). Gray bars indicate the data points that were analyzed for baseline, LP-NPY application, and washout. Black dashed line represents the level of one. Each color represents one cell. The graph was truncated along the *y*-axis to better show the changes observed, removing some of the later responses for the cell in cyan, which ran up during the washout period. Inset, Graph shows the full *y*-axis. ***F***, Graph of normalized data showing that application LP-NPY (500 nM) decreased the area under the curve. Black dashed line represents the level of one, and the dashed gray line represents the level of zero difference for the paired mean difference plot.

uncaging provided functional evidence of local excitatory and inhibitory networks in the IC of young mice (P2–P22; Sturm et al., 2014, 2017). Additionally, a recent study showed that descending input from auditory cortex to the shell IC elicits net inhibitory responses by driving local glutamatergic neurons to activate local networks of GABAergic neurons that in turn synapse broadly onto other shell IC neurons (Oberle et al., 2023). Here, most of our recordings were targeted to central nucleus of the IC, and we found that intrinsic Y_1R^+ projections are very common as only 5 of 54 recorded cells did not receive local inputs from Y_1R^+ neurons. This suggests that Y_1R^+ neurons form much more interconnected networks in the IC than previously expected.

Glutamatergic synapses in the IC often activate both AMPA and NMDA receptors in postsynaptic IC neurons (Ma et al., 2002; Wu et al., 2004; Goyer et al., 2019). Here, we showed that 10 of 14 Y_1R^+ neurons exhibited an NMDA receptor component in their EPSPs at resting membrane potential. This could indicate that local synapses are located on distal dendrites or dendritic spines where activation of AMPA receptors might be sufficient to remove a voltage-dependent Mg^{2+} block of NMDA receptors. However, a recent study from our lab showed that many IC neurons express GluN2C and/or GluN2D NMDA receptor subunits (Drotos et al., 2023), which are relatively insensitive to Mg^{2+} block (Siegler Retchless et al., 2012). Here, recordings that were targeted to Y_1R^- cells, which are likely GABAergic, rarely

←

number of action potentials (***G***) and the area under the curve (***H***) observed in response to light pulses, indicating that LP-NPY inhibited recurrent excitation. Black dashed lines represent the level of one, and dashed gray lines represent the level of zero difference for the paired mean difference plots.

exhibited an NMDA receptor component (one of six cells). The different NMDA receptor expression between Y_1R^+ and Y_1R^- neurons may influence auditory computations in the IC by differently affecting synaptic integration in glutamatergic versus GABAergic neurons (Drotos et al., 2023).

Most synapses undergo dynamic changes during successive release events that result in a temporary increase or decrease in synaptic strength known as short-term synaptic depression or short-term synaptic facilitation. Short-term synaptic plasticity changes the efficacy of a synapse and directly influences neuronal computations, affecting for example, neuronal gain (Dittman et al., 2000; Rothman et al., 2009; Barri et al., 2022). Short-term synaptic plasticity has been widely studied in the central auditory pathway (Friauf et al., 2015; Romero and Trussell, 2021), however, very few studies have been done in the IC (Wu et al., 2004; Kitagawa and Sakaba, 2019). Because axons from multiple sources overlap in the IC, it is challenging to use electrical stimulation to activate single sources of input to IC neurons and even more challenging to separate local from external sources of input. Here, we used optogenetics to selectively stimulate Y_1R^+ neurons in the local IC.

A previous report indicates that lemniscal inputs to IC neurons undergo short-term depression (Wu et al., 2004). This study was conducted using a higher concentration of Ca^{2+} in the ACSF than used here (2.4 mM compared with 1.5 mM Ca^{2+}), which would be expected to enhance short-term depression. However, recent results from our lab using 1.5 mM Ca^{2+} ACSF indicate that ventral cochlear nucleus inputs to the IC undergo short-term synaptic depression (unpublished results). Here, we showed that in contrast to ascending inputs, glutamatergic synapses in the local IC exhibited modest short-term synaptic plasticity, suggesting that synaptic mechanisms in the local IC favor stable synaptic strength at excitatory synapses. When synapses are stimulated at higher frequencies, depletion of the readily releasable pool is likely to occur, causing short-term depression (Zucker and Regehr, 2002). The small changes in EPSP amplitudes during 20 Hz stimulation of Y_1Rs synapses could be explained in two ways. First, it is possible that short-term facilitation compensated for short-term depression, resulting in an increase in release probability (Jackman and Regehr, 2017). Indeed, this balance between short-term depression and short-term facilitation has been shown to be the case in the auditory brainstem of chickens (MacLeod et al., 2007). Second, it is possible that 20 Hz might not be a high enough frequency to result in vesicle depletion. However, in the avian auditory brainstem little short-term synaptic plasticity was observed over a range of different frequencies (MacLeod et al., 2007).

Short-term synaptic plasticity has been hypothesized to contribute to temporal selectivity influencing, for example, sensory adaptation in which the response to a second auditory stimulus is decreased compared with the first stimulus (Phillips et al., 1989; Natan et al., 2017; Motanis et al., 2018; Seay et al., 2020; Valdés-Baizabal et al., 2021). The difference in short-term synaptic plasticity between ascending inputs and local synapses may indicate a shift in the influence from ascending to local synapses during sustained stimuli. Because we used a physiological Ca^{2+} concentration in our ACSF (1.5 mM), it is reasonable to hypothesize that the short-term plasticity reported here is similar to that present under *in vivo* conditions (Borst, 2010), although it should be noted that ongoing patterns of activity *in vivo* will also affect short-term plasticity. We plan to examine short-term plasticity at Y_1R^+ synapses *in vivo* in future studies.

NPY signaling dampens recurrent excitation in the IC

The IC receives several neuromodulatory inputs that mostly come from nonauditory sources outside the IC (Hurley and Pollak, 1999; Motts and Schofield, 2009; Rivera-Perez et al., 2021; Hoyt et al., 2019). Because NPY neurons are located within the IC, NPY signaling is likely to be much more heavily influenced by the ascending auditory pathway than other neuromodulatory inputs to the IC. We previously showed that NPY signaling dampens the excitability of Y_1R^+ neurons (Silveira et al., 2020). Our current results extend this finding by showing that as most glutamatergic IC neurons express Y_1R, NPY is positioned to be a major regulator of excitatory neuronal circuits in the IC.

The importance of NPY signaling has been shown in many brain regions. For example, in the hippocampus, NPY is known as an endogenous antiepileptic agent that decreases excitability during seizures (Colmers and El Bahh, 2003; Giesbrecht et al., 2010). Interestingly, the role of Y_1Rs in modulating seizures in the hippocampus is debated. Some studies suggest that Y_1Rs play a permissive role in seizures (Vezzani et al., 1999) and that the antiepileptic role of NPY is likely to be mediated by presynaptic Y_2Rs (Colmers et al., 1988; Colmers and El Bahh, 2003; Vezzani and Sperk, 2004). Here, we showed that activation of Y_1Rs decreases recurrent excitation in the IC. This contrast could be explained by the fact that in the hippocampus Y_1Rs can be autoreceptors expressed by NPY neurons (Paredes et al., 2003). In the IC, Y_1Rs are expressed in glutamatergic neurons and are not expressed by NPY neurons, which are GABAergic (Silveira et al., 2020). Given that the IC is prone to hyperexcitability (Wei, 2013; Xiong et al., 2017) and that NPY expression in the IC is increased in a rat model of audiogenic seizure (Damasceno et al., 2020), NPY may play a major role in shaping excitatory/inhibitory balance in the IC.

Noise-induced hearing loss can lead to immediate and long-term changes in the activity of IC neurons (Wang et al., 1996; Dong et al., 2010). Noise-induced plasticity in the IC is hypothesized to be a compensatory response to decreased excitatory drive from the periphery (Chambers et al., 2016). This phenomenon is known as enhanced central gain, and when the enhancement goes too far, it can produce maladaptive plasticity that results in clinical conditions such as tinnitus or hyperacusis (Berger and Coomber, 2015; McGill et al., 2022). An increase in action potential frequency generally leads to an increase in neuropeptide release (van den Pol, 2012). Given that noise-induced hearing loss can lead to an overall increase in activity in the central auditory pathway (Manzoor et al., 2012) and that NPY strongly decreases excitability in the IC, it is not unreasonable to think that NPY signaling may limit enhanced gain in the IC after hearing loss. Because GABA and NPY work in different timescales, NPY is likely to modulate network activity in a timescale not possible with GABA alone, therefore complementing GABAergic signaling. In fact, a recent study showed that NPY expression is increased in lateral olivocochlear neurons after noise exposure (Frank et al., 2023). In future studies, we plan to directly assess how NPY signaling contributes to neural plasticity in the IC following noise-induced hearing loss.

Together, our data suggest that NPY signaling is a critical modulator of local circuits in the IC, with potential impacts on auditory computations, central gain control, and plasticity following hearing loss.

References

Adams JC (1979) Ascending projections to the inferior colliculus. J Comp Neurol 183:519–538.

Anair JD, Silveira MA, Mirjalili P, Beebe NL, Schofield BR, Roberts MT (2022) Inhibitory NPY neurons provide a large and heterotopic

commissural projection in the inferior colliculus. Front Neural Circuits 16:871924.
Bacci A, Huguenard JR, Prince DA (2002) Differential modulation of synaptic transmission by neuropeptide Y in rat neocortical neurons. Proc Natl Acad Sci U S A 99:17125–17130.
Barri A, Wiechert MT, Jazayeri M, DiGregorio DA (2022) Synaptic basis of a sub-second representation of time in a neural circuit model. Nat Commun 13:7902.
Bates D, Mächler M, Bolker B, Walker S (2015) Fitting linear mixed-effects models using lme4. J Stat Soft 67:1–48.
Beebe NL, Young JW, Mellott JG, Schofield BR (2016) Extracellular molecular markers and soma size of inhibitory neurons: evidence for four subtypes of GABAergic cells in the inferior colliculus. J Neurosci 36:3988–3999.
Berger JI, Coomber B (2015) Tinnitus-related changes in the inferior colliculus. Front Neurol 6:61.
Bernard C (2019) Changing the way we report, interpret, and discuss our results to rebuild trust in our research. eNeuro 6:ENEURO.0259-19.2019.
Borst JGG (2010) The low synaptic release probability *in vivo*. Trends Neurosci 33:259–266.
Burke DA, Rotstein HG, Alvarez VA (2017) Striatal local circuitry: a new framework for lateral inhibition. Neuron 96:267–284.
Calin-Jageman RJ (2022) Better inference in neuroscience: test less, estimate more. J Neurosci 42:8427–8431.
Calin-Jageman RJ, Cumming G (2019) Estimation for better inference in neuroscience. eNeuro 6:ENEURO.0205-19.2019.
Cant NB, Benson CG (2006) Organization of the inferior colliculus of the gerbil (*Meriones unguiculatus*): differences in distribution of projections from the cochlear nuclei and the superior olivary complex. J Comp Neurol 495:511–528.
Cant NB, Benson CG (2007) Multiple topographically organized projections connect the central nucleus of the inferior colliculus to the ventral division of the medial geniculate nucleus in the gerbil, *Meriones unguiculatus*. J Comp Neurol 503:432–453.
Chambers AR, Resnik J, Yuan Y, Whitton JP, Edge AS, Liberman MC, Polley DB (2016) Central gain restores auditory processing following near-complete cochlear denervation. Neuron 89:867–879.
Chen C, Cheng M, Ito T, Song S (2018) Neuronal organization in the inferior colliculus revisited with cell-type-dependent monosynaptic tracing. J Neurosci 38:3318–3332.
Colmers WF, Bleakman D (1994) Effects of neuropeptide Y on the electrical properties of neurons. Trends Neurosci 17:373–379.
Colmers WF, El Bahh B (2003) Neuropeptide Y and epilepsy. Epilepsy Curr 3:53–58.
Colmers WF, Lukowiak K, Pittman QJ (1988) Neuropeptide Y action in the rat hippocampal slice: site and mechanism of presynaptic inhibition. J Neurosci 8:3827–3837.
Damasceno S, Gómez-Nieto R, Garcia-Cairasco N, Herrero-Turrión MJ, Marín F, Lopéz DE (2020) Top common differentially expressed genes in the epileptogenic nucleus of two strains of rodents susceptible to audiogenic seizures: WAR and GASH/Sal. Front Neurol 11:33.
Dittman JS, Kreitzer AC, Regehr WG (2000) Interplay between facilitation, depression, and residual calcium at three presynaptic terminals. J Neurosci 20:1374–1385.
Dong S, Mulders WHAM, Rodger J, Woo S, Robertson D (2010) Acoustic trauma evokes hyperactivity and changes in gene expression in guinea-pig auditory brainstem. Eur J Neurosci 31:1616–1628.
Drotos A, Herrera Y, Zarb R, Roberts M (2023) GluN2D-containing NMDA receptors enhance temporal integration in VIP neurons in the inferior colliculus. bioRxiv 538607. https://doi.org/10.1101/2023.04.27.538607.
Dumont Y, Jacques D, Bouchard P, Quirion R (1998) Species differences in the expression and distribution of the neuropeptide Y Y1, Y2, Y4, and Y5 receptors in rodents, guinea pig, and primates brains. J Comp Neurol 402:372–384.
Eva C, Serra M, Mele P, Panzica G, Oberto A (2006) Physiology and gene regulation of the brain NPY Y1 receptor. Front Neuroendocrinol 27:308–339.
Frank MM, Sitko AA, Suthakar K, Torres Cadenas L, Hunt M, Yuk MC, Weisz CJC, Goodrich LV (2023) Experience-dependent flexibility in a molecularly diverse central-to-peripheral auditory feedback system. Elife 12:e83855.
Friauf E, Fischer AU, Fuhr MF (2015) Synaptic plasticity in the auditory system: a review. Cell Tissue Res 361:177–213.
Fu L-Y, Acuna-Goycolea C, van den Pol AN (2004) Neuropeptide Y inhibits hypocretin/orexin neurons by multiple presynaptic and postsynaptic mechanisms: tonic depression of the hypothalamic arousal system. J Neurosci 24:8741–8751.
Geiller T, Sadeh S, Rolotti SV, Blockus H, Vancura B, Negrean A, Murray AJ, Rózsa B, Polleux F, Clopath C, Losonczy A (2022) Local circuit amplification of spatial selectivity in the hippocampus. Nature 601:105–109.
Giesbrecht CJ, Mackay JP, Silveira HB, Urban JH, Colmers WF (2010) Countervailing modulation of Ih by neuropeptide Y and corticotrophin-releasing factor in basolateral amygdala as a possible mechanism for their effects on stress-related behaviors. J Neurosci 30:16970–16982.
Glass MJ, Chan J, Pickel VM (2002) Ultrastructural localization of neuropeptide Y Y1 receptors in the rat medial nucleus tractus solitarius: relationships with neuropeptide Y or catecholamine neurons. J Neurosci Res 67:753–765.
Gøtzsche CR, Woldbye DPD (2016) The role of NPY in learning and memory. Neuropeptides 55:79–89.
Goyer D, Silveira MA, George AP, Beebe NL, Edelbrock RM, Malinski PT, Schofield BR, Roberts MT (2019) A novel class of inferior colliculus principal neurons labeled in vasoactive intestinal peptide-Cre mice. Elife 8:e43770.
Gutman AR, Yang Y, Ressler KJ, Davis M (2008) The role of neuropeptide Y in the expression and extinction of fear-potentiated startle. J Neurosci 28:12682–12690.
Ho J, Tumkaya T, Aryal S, Choi H, Claridge-Chang A (2019) Moving beyond P values: data analysis with estimation graphics. Nat Methods 16:565–566.
Hothorn T, Hornik K, van de Wiel M, Zeileis A (2006) A Lego system for conditional inference. Am Stat 60:257–263.
Hothorn T, Hornik K, van de Wiel M, Zeileis A (2008) Implementing a class of permutation tests: the coin package. J Stat Soft 28:1–23.
Hoyt JM, Perkel DJ, Portfors CV (2019) Dopamine acts via D2-like receptors to modulate auditory responses in the inferior colliculus. eNeuro 6:ENEURO.0350-19.2019.
Hurley LM, Pollak GD (1999) Serotonin differentially modulates responses to tones and frequency-modulated sweeps in the inferior colliculus. J Neurosci 19:8071–8082.
Ito T, Bishop DC, Oliver DL (2011) Expression of glutamate and inhibitory amino acid vesicular transporters in the rodent auditory brainstem. J Comp Neurol 519:316–340.
Ito T, Bishop DC, Oliver DL (2016) Functional organization of the local circuit in the inferior colliculus. Anat Sci Int 91:22–34.
Jackman SL, Regehr WG (2017) The mechanisms and functions of synaptic facilitation. Neuron 94:447–464.
Kim J, Alger BE (2001) Random response fluctuations lead to spurious paired-pulse facilitation. J Neurosci 21:9608–9618.
Kitagawa M, Sakaba T (2019) Developmental changes in the excitatory short-term plasticity at input synapses in the rat inferior colliculus. Eur J Neurosci 50:2830–2846.
Klapoetke NC, et al. (2014) Independent optical excitation of distinct neural populations. Nat Methods 11:338–346.
Kopp J, Xu Z-Q, Zhang X, Pedrazzini T, Herzog H, Kresse A, Wong H, Walsh JH, Hökfelt T (2002) Expression of the neuropeptide Y Y1 receptor in the CNS of rat and of wild-type and Y1 receptor knock-out mice. Focus on immunohistochemical localization. Neuroscience 111:443–532.
Kreeger LJ, Connelly CJ, Mehta P, Zemelman BV, Golding NL (2021) Excitatory cholecystokinin neurons of the midbrain integrate diverse temporal responses and drive auditory thalamic subdomains. Proc Natl Acad Sci U S A 118:e2007724118.
Li Q, Bartley AF, Dobrunz LE (2017) Endogenously released neuropeptide Y suppresses hippocampal short-term facilitation and is impaired by stress-induced anxiety. J Neurosci 37:23–37.
Ma CL, Kelly JB, Wu SH (2002) AMPA and NMDA receptors mediate synaptic excitation in the rat's inferior colliculus. Hear Res 168:25–34.
MacLeod KM, Horiuchi TK, Carr CE (2007) A role for short-term synaptic facilitation and depression in the processing of intensity information in the auditory brain stem. J Neurophysiol 97:2863–2874.
Madisen L, Zwingman TA, Sunkin SM, Oh SW, Zariwala HA, Gu H, Ng LL, Palmiter RD, Hawrylycz MJ, Jones AR, Lein ES, Zeng H (2010) A robust

and high-throughput Cre reporting and characterization system for the whole mouse brain. Nat Neurosci 13:133–140.

Manzoor NF, Licari FG, Klapchar M, Elkin RL, Gao Y, Chen G, Kaltenbach JA (2012) Noise-induced hyperactivity in the inferior colliculus: its relationship with hyperactivity in the dorsal cochlear nucleus. J Neurophysiol 108:976–988.

Mardinly AR, Oldenburg IA, Pégard NC, Sridharan S, Lyall EH, Chesnov K, Brohawn SG, Waller L, Adesnik H (2018) Precise multimodal optical control of neural ensemble activity. Nat Neurosci 21:881–893.

McGill M, Hight AE, Watanabe YL, Parthasarathy A, Cai D, Clayton K, Hancock KE, Takesian A, Kujawa SG, Polley DB (2022) Neural signatures of auditory hypersensitivity following acoustic trauma. Elife 11: e80015.

Motanis H, Seay MJ, Buonomano DV (2018) Short-term synaptic plasticity as a mechanism for sensory timing. Trends Neurosci 41:701–711.

Motts SD, Schofield BR (2009) Sources of cholinergic input to the inferior colliculus. Neuroscience 160:103–114.

Natan RG, Rao W, Geffen MN (2017) Cortical interneurons differentially shape frequency tuning following adaptation. Cell Rep 21:878–890.

Nelson TS, Fu W, Donahue RR, Corder GF, Hökfelt T, Wiley RG, Taylor BK (2019) Facilitation of neuropathic pain by the NPY Y1 receptor-expressing subpopulation of excitatory interneurons in the dorsal horn. Sci Rep 9:7248.

Noben-Trauth K, Zheng QY, Johnson KR (2003) Association of cadherin 23 with polygenic inheritance and genetic modification of sensorineural hearing loss. Nat Genet 35:21–23.

Oberle HM, Ford AN, Czarny JE, Rogalla MM, Apostolides PF (2023) Recurrent circuits amplify corticofugal signals and drive feedforward inhibition in the inferior colliculus. J Neurosci 43:5642–5655.

Oliver DL, Kuwada S, Yin TC, Haberly LB, Henkel CK (1991) Dendritic and axonal morphology of HRP-injected neurons in the inferior colliculus of the cat. J Comp Neurol 303:75–100.

Oliver DL, Winer JA, Beckius GE, Saint Marie RL (1994) Morphology of GABAergic neurons in the inferior colliculus of the cat. J Comp Neurol 340:27–42.

Ono M, Yanagawa Y, Koyano K (2005) GABAergic neurons in inferior colliculus of the GAD67-GFP knock-in mouse: electrophysiological and morphological properties. Neurosci Res 51:475–492.

Padilla SL, Qiu J, Soden ME, Sanz E, Nestor CC, Barker FD, Quintana A, Zweifel LS, Rønnekleiv OK, Kelly MJ, Palmiter RD (2016) Agouti-related peptide neural circuits mediate adaptive behaviors in the starved state. Nat Neurosci 19:734–741.

Palmer AR, Shackleton TM, Sumner CJ, Zobay O, Rees A (2013) Classification of frequency response areas in the inferior colliculus reveals continua not discrete classes. J Physiol 591:4003–4025.

Paredes MF, Greenwood J, Baraban SC (2003) Neuropeptide Y modulates a G protein-coupled inwardly rectifying potassium current in the mouse hippocampus. Neurosci Lett 340:9–12.

Peruzzi D, Bartlett E, Smith PH, Oliver DL (1997) A monosynaptic GABAergic input from the inferior colliculus to the medial geniculate body in rat. J Neurosci 17:3766–3777.

Peruzzi D, Sivaramakrishnan S, Oliver DL (2000) Identification of cell types in brain slices of the inferior colliculus. Neuroscience 101:403–416.

Petreanu L, Mao T, Sternson SM, Svoboda K (2009) The subcellular organization of neocortical excitatory connections. Nature 457:1142–1145.

Phillips DP, Hall SE, Hollett JL (1989) Repetition rate and signal level effects on neuronal responses to brief tone pulses in cat auditory cortex. J Acoust Soc Am 85:2537–2549.

Reetz G, Ehret G (1999) Inputs from three brainstem sources to identified neurons of the mouse inferior colliculus slice. Brain Res 816:527–543.

Rivera-Perez LM, Kwapiszewski JT, Roberts MT (2021) $\alpha 3\beta 4^*$ Nicotinic acetylcholine receptors strongly modulate the excitability of VIP neurons in the mouse inferior colliculus. Front Neural Circuits 15:709387.

Romero GE, Trussell LO (2021) Distinct forms of synaptic plasticity during ascending vs descending control of medial olivocochlear efferent neurons. Elife 10:e66396.

Roseberry AG, Liu H, Jackson AC, Cai X, Friedman JM (2004) Neuropeptide Y-mediated inhibition of proopiomelanocortin neurons in the arcuate nucleus shows enhanced desensitization in ob/ob mice. Neuron 41: 711–722.

Rostkowski AB, Teppen TL, Peterson DA, Urban JH (2009) Cell-specific expression of neuropeptide Y Y1 receptor immunoreactivity in the rat basolateral amygdala. J Comp Neurol 517:166–176.

Rothman JS, Cathala L, Steuber V, Silver RA (2009) Synaptic depression enables neuronal gain control. Nature 457:1015–1018.

Saka E, Iadarola M, Fitzgerald DJ, Graybiel AM (2002) Local circuit neurons in the striatum regulate neural and behavioral responses to dopaminergic stimulation. Proc Natl Acad Sci U S A 99:9004–9009.

Saldaña E, Merchán M (2005) Intrinsic and commissural connections of the inferior colliculus. In: The inferior colliculus (Winer JA, Schreiner CE, eds), pp 155–176. New York: Springer.

Schindelin J, Arganda-Carreras I, Frise E, Kaynig V, Longair M, Pietzsch T, Preibisch S, Rueden C, Saalfeld S, Schmid B, Tinevez J-Y, White DJ, Hartenstein V, Eliceiri K, Tomancak P, Cardona A (2012) Fiji: an open-source platform for biological-image analysis. Nat Methods 9:676–682.

Seay MJ, Natan RG, Geffen MN, Buonomano DV (2020) Differential short-term plasticity of PV and SST neurons accounts for adaptation and facilitation of cortical neurons to auditory tones. J Neurosci 40:9224–9235.

Siegler Retchless B, Gao W, Johnson JW (2012) A single GluN2 subunit residue controls NMDA receptor channel properties via intersubunit interaction. Nat Neurosci 15:406–413.

Silveira MA, Anair JD, Beebe NL, Mirjalili P, Schofield BR, Roberts MT (2020) Neuropeptide Y expression defines a novel class of GABAergic projection neuron in the inferior colliculus. J Neurosci 40:4685–4699.

Sivaramakrishnan S, Oliver DL (2001) Distinct K currents result in physiologically distinct cell types in the inferior colliculus of the rat. J Neurosci 21:2861–2877.

Strasser H, Weber CU (1999) On the asymptotic theory of permutation statistics. Vienna University of Economics and Business: Report Series SFB Adaptive Information Systems and Modelling in Economics and Management Science No. 27.

Sturm J, Nguyen T, Kandler K (2014) Development of intrinsic connectivity in the central nucleus of the mouse inferior colliculus. J Neurosci 34: 15032–15046.

Sturm JJ, Zhang-Hooks Y-X, Roos H, Nguyen T, Kandler K (2017) Noise trauma-induced behavioral gap detection deficits correlate with reorganization of excitatory and inhibitory local circuits in the inferior colliculus and are prevented by acoustic enrichment. J Neurosci 37:6314–6330.

Sun QQ, Akk G, Huguenard JR, Prince DA (2001a) Differential regulation of GABA release and neuronal excitability mediated by neuropeptide Y1 and Y2 receptors in rat thalamic neurons. J Physiol 531:81–94.

Sun QQ, Huguenard JR, Prince DA (2001b) Neuropeptide Y receptors differentially modulate G-protein-activated inwardly rectifying K+ channels and high-voltage-activated Ca^{2+} channels in rat thalamic neurons. J Physiol 531:67–79.

Tu B, Timofeeva O, Jiao Y, Nadler JV (2005) Spontaneous release of neuropeptide Y tonically inhibits recurrent mossy fiber synaptic transmission in epileptic brain. J Neurosci 25:1718–1729.

Valdés-Baizabal C, Casado-Román L, Bartlett EL, Malmierca MS (2021) *In vivo* whole-cell recordings of stimulus-specific adaptation in the inferior colliculus. Hear Res 399:107978.

van den Pol AN (2012) Neuropeptide transmission in brain circuits. Neuron 76:98–115.

van den Pol AN, Yao Y, Fu L-Y, Foo K, Huang H, Coppari R, Lowell B, Broberger C (2009) Neuromedin B and gastrin-releasing peptide excite arcuate nucleus neuropeptide Y neurons in a novel transgenic mouse expressing strong renilla green fluorescent protein in NPY neurons. J Neurosci 29:4622–4639.

Vezzani A, Sperk G (2004) Overexpression of NPY and Y2 receptors in epileptic brain tissue: an endogenous neuroprotective mechanism in temporal lobe epilepsy? Neuropeptides 38:245–252.

Vezzani A, Sperk G, Colmers WF (1999) Neuropeptide Y: emerging evidence for a functional role in seizure modulation. Trends Neurosci 22:25–30.

Vollmer LL, Schmeltzer S, Schurdak J, Ahlbrand R, Rush J, Dolgas CM, Baccei ML, Sah R (2016) Neuropeptide Y impairs retrieval of extinguished fear and modulates excitability of neurons in the infralimbic prefrontal cortex. J Neurosci 36:1306–1315.

Wahlestedt C, Yanaihara N, Håkanson R (1986) Evidence for different pre- and post-junctional receptors for neuropeptide Y and related peptides. Regul Pept 13:307–318.

Wang F, Flanagan J, Su N, Wang L-C, Bui S, Nielson A, Wu X, Vo H-T, Ma X-J, Luo Y (2012) RNAscope: a novel in situ RNA analysis platform for formalin-fixed, paraffin-embedded tissues. J Mol Diagn JMD 14:22–29.

Wang J, Salvi RJ, Powers N (1996) Plasticity of response properties of inferior colliculus neurons following acute cochlear damage. J Neurophysiol 75:171–183.

Wei S (2013) Peripheral hearing loss causes hyperexcitability of the inferior colliculus. J Otol 8:39–43.

Winer JA, Saint Marie RL, Larue DT, Oliver DL (1996) GABAergic feedforward projections from the inferior colliculus to the medial geniculate body. Proc Natl Acad Sci U S A 93:8005–8010.

Wittmann G, Hrabovszky E, Lechan RM (2013) Distinct glutamatergic and GABAergic subsets of hypothalamic pro-opiomelanocortin neurons revealed by *in situ* hybridization in male rats and mice. J Comp Neurol 521:3287–3302.

Wu SH, Ma CL, Kelly JB (2004) Contribution of AMPA, NMDA, and GABA (A) receptors to temporal pattern of postsynaptic responses in the inferior colliculus of the rat. J Neurosci 24:4625–4634.

Xiong B, Alkharabsheh A, Manohar S, Chen G-D, Yu N, Zhao X, Salvi R, Sun W (2017) Hyperexcitability of inferior colliculus and acoustic startle reflex with age-related hearing loss. Hear Res 350:32–42.

Zucker RS, Regehr WG (2002) Short-term synaptic plasticity. Annu Rev Physiol 64:355–405.